Supplementary Information for:

Fluorinated Metal Organic Frameworks, MFFIVE-Ni-L (M=Fe/Al, L=pyr), with Coordinatively Unsaturated Metal Site for CO$_2$ Separation from Flue Gas Composition in presence of Humidity by Computational Methods

Athulya S. Palakkal and Renjith S. Pillai*

Department of Chemistry, Faculty of Engineering and Technology, SRM Institute of Science and Technology, Kattankulathur-603 203, Chennai, India

Email: renjiths@srmist.edu.in / renjithspillai@gmail.com

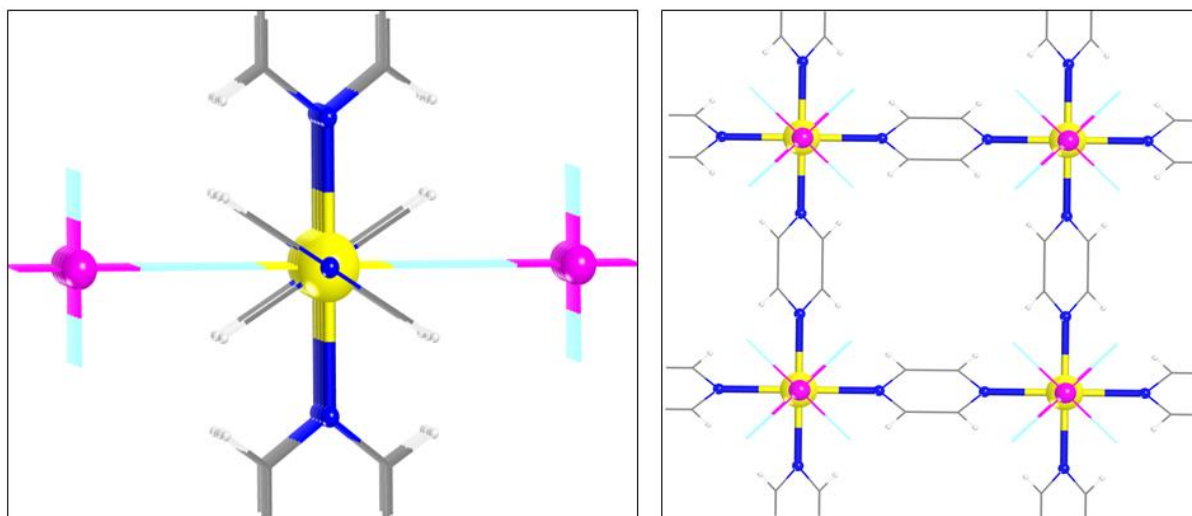# 1. Crystalline Structures of FEFFIVE with Pyrazine organic linker

Fig. S1. Crystal structures extracted from experimental X-ray diffraction measurements for FEFFIVE-Ni-Pyr[1], unit cell (1×1×1) and super cell (2×2×2) viewed along c and direction, respectively. (Color code: Ni, yellow; Fe, violet; F, blue; C, gray; N, blue; H, white).

2. Microscopic models for the host [Ni (pyrazine)$_2$(FeF$_5$)$_n$] framework.

2.1. Optimization of dry crystal structure.

As consistent with the experimental assessment of the structural symmetry of the solid, the initial symmetry of [Ni(pyrazine)$_2$(FeF$_5$)$_n$] MOF corresponds to a tetragonal bipyramidal geometry[1]. This MOF is optimized using PBE[2,3] Density Functional Theory (DFT) functional by employing CP2K[4-7] package. The electronic system customarily discussed with the help of Hubbard function.[8]The GGA+U approach made an improvisation to describe the ground state of d-electron system[9,10]. Additionally, used spin-unrestricted Kohn-Sham (UKS) method for the spin polarization to perform ligand-metal interaction.[11]This model is able to approximate the electron pair correlation function. The elements present in the MOF such as Carbon, Oxygen, Nitrogen, Fluorine and Hydrogen, a triple zeta (TZVP-MOLOPT)[12] basis set was considered, for the Iron and Nickel a double zeta (DZVP-MOLOPT)[12]was applied. The CUS-MOF [Ni(pyrazine)$_2$(FeF$_5$)n] (here after FEFFIVE-Ni-pyr-TB) also compared with the previously optimized isostructure, [Ni(pyrazine)$_2$(AlF$_5$)n], (hereafter ALFFIVE-Ni-pyr-TB)[13].The optimized unit cell parameters for these structures are reported in Table S1.

Table S1. Cell parameters ofFEFFIVE-Ni-pyr-TB and ALFFIVE-Ni-pyr-TB[13,14], obtained by DFT optimization (Dry case).

MOF	Lattice Size(Å)			Angle (^{0})			Cell volume (Å^3)	Energy (eV)
	a	**b**	**c**	**α**	**β**	**γ**		
FEFFIVE-Ni-Pyr-TB	7.007	7.007	7.929	90	90	90	389.298	-13721.91
ALFFIVE-Ni-pyr-TB[13,14]	6.901	6.901	8.015	90	90	90	381.705	-10416.85

2.2. Optimization of H_2O-loaded Crystalline [Ni(pyrazine)$_2$(FeF$_5$)n]

The saturated water loading capacity for the [Ni(pyrazine)$_2$(FeF$_5$)n] and [Ni(pyrazine)$_2$(AlF$_5$)n] is ~22.0 wt% (i.e. 5 H_2O/u.c) and 15.85wt% (i.e. 3 H_2O/u.c) respectively as observed from the experimental water adsorption isotherm[1]. The experimentally obtained saturated capacities of H_2O were randomly loaded into the optimized dry FEFFIVE-Ni-pyr-TB structure using Material Studio Software suite[15] and further these H_2O-loaded structures were considered for geometry optimization.These simulations were performed using CP2K package[4-7] at the DFT-level keeping the same functional and basis set used for the dry structure, where (i) the positions of both the atoms of the MOF framework and the H_2O molecules, and (ii) its cell parameters were fully relaxed. The trigonal bipyramidal geometry of FeF$_5$ is changed to square bipyramidal FeF$_5$H$_2$O upon the optimization of FEFFIVE-Ni-pyr-TB with saturated water. The DFT-optimized H_2O-loaded FEFFIVE-Ni-pyr-TB is denoted as FEFFIVE-Ni-pyr-SB. The optimized unit cell parameters and slected geometrical parameters for FEFFIVE-Ni-pyr-SBand its isostructural previously DFT-optimized ALFFIVE-Ni-pyr-SB[14]structures are reported in Table S2 and S3.The atomic partial charges of all the atoms are calculated by using REPEAT method [16](Table S5). In addition to these water molecules per unit cell was progressively added into the FEFFIVE-Ni-pyr-TB models, and further optimized the 1, 2, 3, 4, 5 and 7 H_2O/u c loaded FEFFIVE-Ni-pyr-TB with the same level of theory as used above.

Table S2. Cell parameters of H_2O loaded FEFFIVE-Ni-pyr-SB and ALFFIVE-Ni-pyr-SB obtained by DFT optimization.

MOF	Lattice Size(Å)			Angle (^{0})			Cell volume(A^0)^3	Energy (eV)
	a	**b**	**c**	**α**	**β**	**γ**		
FEFFIVE-Ni-Pyr-SB	7.063	7.063	7.888	90.00	90.00	90.00	393.501	-15599.69
ALFFIVE-Ni-py-SB[14]	6.871	6.871	8.364	90.00	90.00	90.00	394.870	-11824.66

Table S3. Experimental and simulated bond length and unit cell dimensions.

	FEFFIVE-Ni-pyr-SB	
Bond	Experimental[1] (Å)	Simulated (Å)
Fe-F$_{equ}$	1.937	1.618
Fe-F$_{axial}$	1.951	1.789
Ni-F$_{axial}$	2.034	2.145
Ni-N	2.107	2.080
Fe-O	1.890	1.604
C-H	0.930	1.060
a=b	9.892	7.063
c	7.971	7.888

Table S4. The possible distance of step by step of water loading optimized structure of FEFFIVE-Ni-pyr

No. of Water loaded in FEFFIVE-Ni-pyr	Distance of H$_{H2O}$-H$_{organic}$ (Å)	Distance of O$_{H2O}$-N$_{Pyrazine}$ (Å)	Distance of O$_{H2O}$-Fe (Å)
1H$_2$O	2.490	4.609	4.412
2H$_2$O	2.530	4.317	4.392
3H$_2$O	3.080	4.392	3.419
4H$_2$O	1.470	2.722	3.728
5H$_2$O	1.537	2.347	1.604
6H$_2$O	1.483	3.735	1.703
7H$_2$O	1.508	3.755	1.717

Table S5. Atomic partial charges of FEFFIVE-Ni-pyr-TB structure

Atomic types	C1a	C2a	F1	F2	H1a	H2a	Ni	N1a	Fe
Charge (e)	-0.121	-0.125	-0.401	-0.372	0.168	0.169	0.099	-0.111	1.899

3. Pore size distribution, pore volume, specific surface area calculations.

The pore size distributions (PSD)[17] of optimized FEFFIVE-Ni-pyr and ALFFIVE-Ni-pyr with and without H_2O loaded were calculated by Gelb and Gubbins[18] methodology, as shown in Fig. S2. Moreover, internal surface area and pore volume is taken to account. In which the internal surface area calculated through the random selection and checking the point of overlap. While the estimation of pore volume based on the insertion of a random point and checking the overlap and fractionalized with the total attempted movement. These strategies are outline through Gelb and Gubbins[18] methodology (Table S6).

Table S6. Surface area and Pore volume of MFFIVE-Ni-pyr-TB/SB M=FE/AL.

	FEFFIVE-Ni-pyr-TB	ALFFIVE-Ni-pyr-TB	FEFFIVE-Ni-pyr-SB	ALFFIVE-Ni-pyr-SB
Surface Area(m^2/g)	1034.5	1032.4	1549.9	1947.8
Pore volume(cc/g) (Free volume)	0.1470	0.1462	0.1810	0.2399
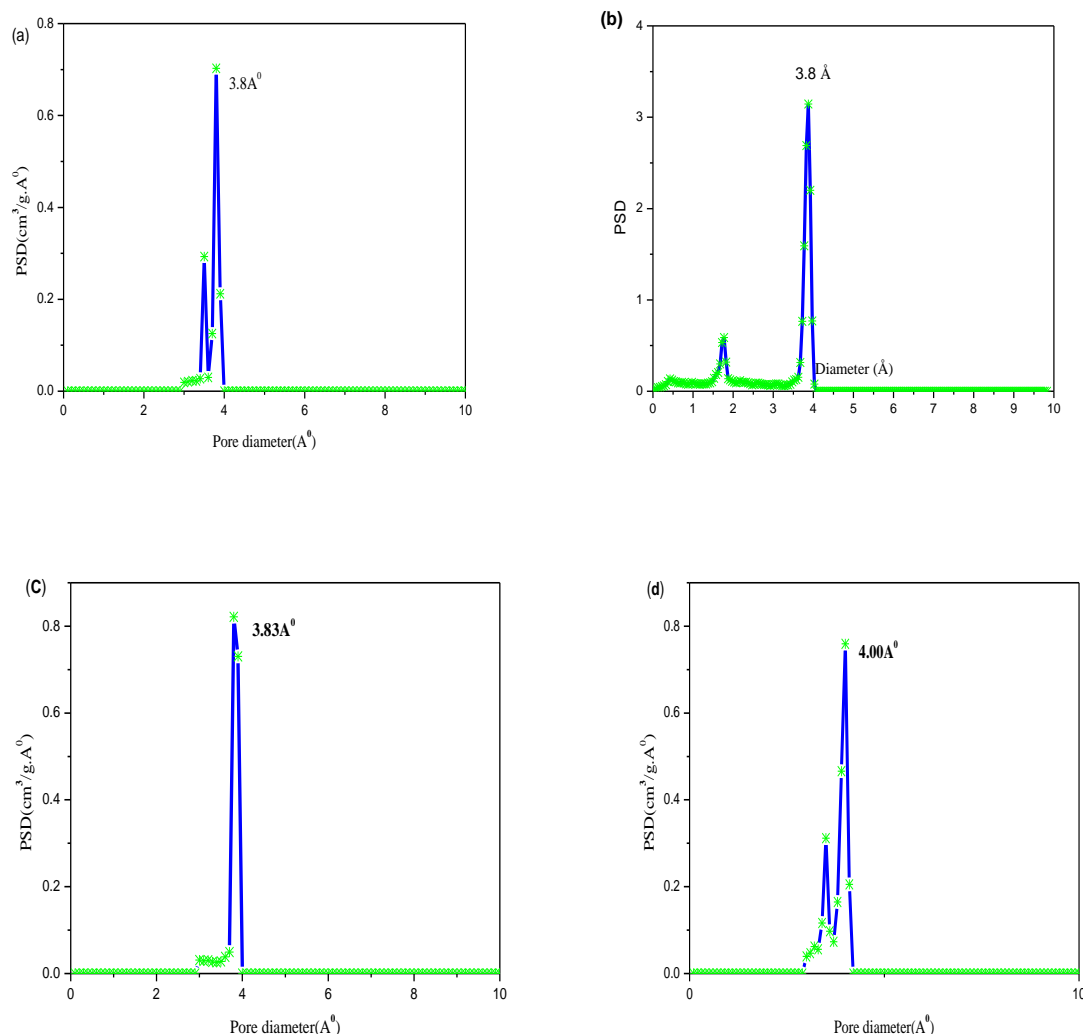
Fig. S2. Pore size distributions for optimized structures of dry (a) FEFFIVE-Ni-pyr-TB (b) ALFFIVE-Ni-pyr-TB and H_2O loaded structure of (c) FEFFIVE-Ni-pyr-SB and (d) ALFFIVE-Ni-pyr-SB.

4. Interatomic Potentials (Generic Force field).

Initially, the overall interaction between the MOFs and guest molecules were modelled via combination of Lennard-jones and coulombic term (reported in Table S7). The LJ parameters are clarified by using Universal force field (UFF)[19] and DREIDING[20] potentials for respective inorganic and organic part of the atoms in the MOF framework, except for Al which is considered from Faro et .al[13]. In this work, CO_2 adsorbate models were initially considered by EPM2[21], EPM[21], TraPPE[22] intermolecular potential, N_2 by TraPPE[22], MOM[23] and Murad et al three site model[24] and H_2O by TIP4P2005[25,26], TIP4PEw [27] ,SPCE[28], TIP5P[29] and TIP4P[30] respectively .

Table S7. LJ potential parameters forthe atoms of the MFFIVE-Ni-pyr series.

Atomic type	LJ	
	σ (Å)	ε /k_B(K)
C	3.473	47.857
H	2.846	7.649
N	3.662	34.724
F	3.093	38.975
Ni	2.8340	7.5483
Fe	2.9120	6.5419
Al	1.447	108.998

Table S8. Potential parameters and partial charges for the adsorbates

Model	Atomic type	σ (Å)	ε /k_B(K)	q(e)
TraPPE[22]	N2_N	3.310	36.000	-0.4820
	N2_COM	0.00	0.00	0.9640
MOM[23]	N2_N	4.307	99.6381	-0.4050
Three site model[24]	N2_N	3.05	36.4332	0.40484
EPM2[21]	CO2_C	2.757	28.129	0.6512
	CO2_O	3.033	80.507	-0.3256
TraPPE[22]	CO2_C	2.80	27.0	0.7000
	CO2_O	3.05	79.0	-0.3500
EPM[21]	CO2_C	2.785	28.99	0.6645
	CO2_O	2.921	49.060	-0.3322
TIP4P2005[25,26]	O_e	3.159	93.2	0.0000
	M_e	0.00	0.00	-1.1128
TIP4PEw[27]	O_e	3.1643	81.8743	0.000
	M_e	0.00	0.0	-1.0484
SPCE[28]	O_e	3.166	327.095	0.000
	M_e	0.0	0.0	-0.8746
TIP5P[29]	O_e	3.1200	336.8578	0.000
	M_e	0.0	0.0	-0.2410
TIP4P[30]	O_e	3.153	326.088	0.000
	M_e	0.0	0.0	-1.04

6. GCMC Simulations.

Grand Canonical Monte Carlo (GCMC) simulations were carried out to predict the single component adsorption of gases, H_2O, CO_2 and N_2, and co-adsorption of CO_2/N_2 and $CO_2/N_2/H_2O$ in all the DFT-optimized structures, FEFFIVE-Ni-pyr-TB, ALFFIVE-Ni-pyr-TB, FEFFIVE-Ni-pyr-SB, and ALFFIVE-Ni-pyr-SB, at 298 K by employing the RASPA[31] simulation code.We also conducted ternary adsorption of $H_2O/CO_2/N_2$, in which simply assume that N_2 does adsorb negligibly at these conditions from their bulk mole fraction (85%).Our simplified flue gases are at total pressure of 1.0 bar at temperature of 298 K with a range of H_2O mole fraction varying from 0.001% to 0.5%.(E.g. 0.01% H_2O, 14.99% CO_2, and 85% N_2 at 1bar, T =298K) with various adsorbate models.The simulation boxes were made of (4×4×4) 64 unit cells. In the guest-host interaction the short range dispersion force define through LJ potential and long range electrostatic interaction via Ewald summation technique. The LJ is truncated and lifted to zero by 12 Å. In the given thermodynamic conditions the fugacities of adsorbed species are calculated through Peng- Robinson equation of states (EoS)[32]. For each state point, 2×10^8 and 5×10^7 Monte Carlo steps have been employed for equilibration and production runs, respectively. Three types of trials were considered for the molecules: (i) translation or rotation, (ii) creation / deletion and (iii) exchange of molecular identity. In addition to this, the translation and rotation Monte Carlo steps were only allowed for pre-loaded H_2O during the GCMC simulation for simulated co-adsorption under pre-humidified conditions. The adsorption enthalpy at low coverage (Δh) for each gas was calculated through configurational-bias Monte Carlo simulations performed in the NVT ensemble using the revised Widom's test particle insertion method.[33]

6.1 Adsorbent selection criteria

There is a number of benchmarks are available to determine the characteristic and performance of an adsorbent in the adsorption process, currently we chosen selectivity (S) of CO_2 over N_2, working capacity (ΔN) and Adsorption Performance Indicator (API)to account the adsorbent performance.

In this work, selectivity of CO_2 over N_2 with the mole fraction of flue gases in power plant is used (15 % CO_2 and 85 % N_2),

$$S(CO_2/N_2) = (x_{co_2}/x_{N_2})(y_{N_2}/y_{CO_2}) \qquad (1)$$

Where x_{co2} and x_{N2} represents the mole fraction of CO_2 and N_2 in the adsorbed phase and y_{N_2} and y_{CO_2} represents the mole fraction of N_2 and CO_2 in bulk phase respectively. The calculated selectivity's are shown in the TableS9.

One of the important parameter used in the basic application of selecting the adsorbent is carried out mainly via on working capacity (ΔN)[34,35].It is determined through the distinction of gas uptake at the stage of high pressure(N_H) and lower pressure (N_L), generally expressed as the unit of cc/cc adsorbent (Table S10).

$$(\Delta N) = N_H - N_L \qquad (2)$$

Moreover, one of the significant parameter known as Adsorption Performance Indicator (API) proposed by Wiersum et al.[35] to analyse the performance in MOFs,

$$API = (S_{12} - 1)^A * \frac{\Delta N^B}{\Delta H^C} \qquad (3)$$

Where the S_{12}corresponds to the selectivity of highly adsorbed to least adsorbed, ΔN is the working capacity of highly adsorbed species and ΔH terms the average enthalpy of adsorbed species. Here all the A, B, C components used to be one, because of the objective of separation.

7. Comparison of the single component isotherms in dry MFFIVE-Ni-pyr-TB (M=FE/AL).
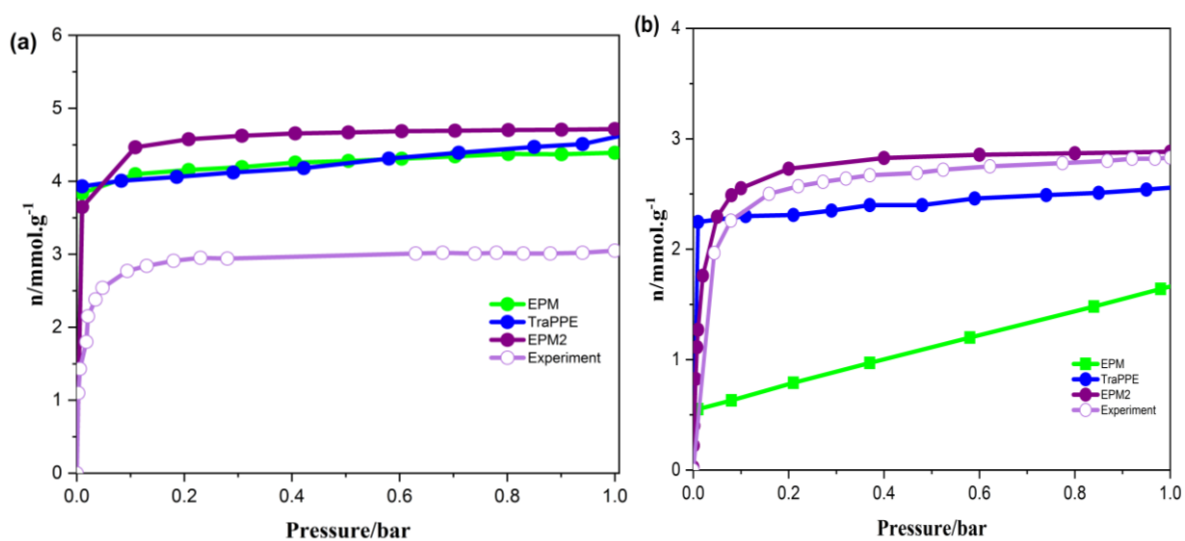
Fig. S3. Single component adsorption isotherm for simulated (closed) using general force field and experimental (open) CO_2 by DFT-optimized dry structures FEFFIVE-Ni-pyr-TB (a) and ALFFIVE-Ni-pyr-TB (b) at 298K
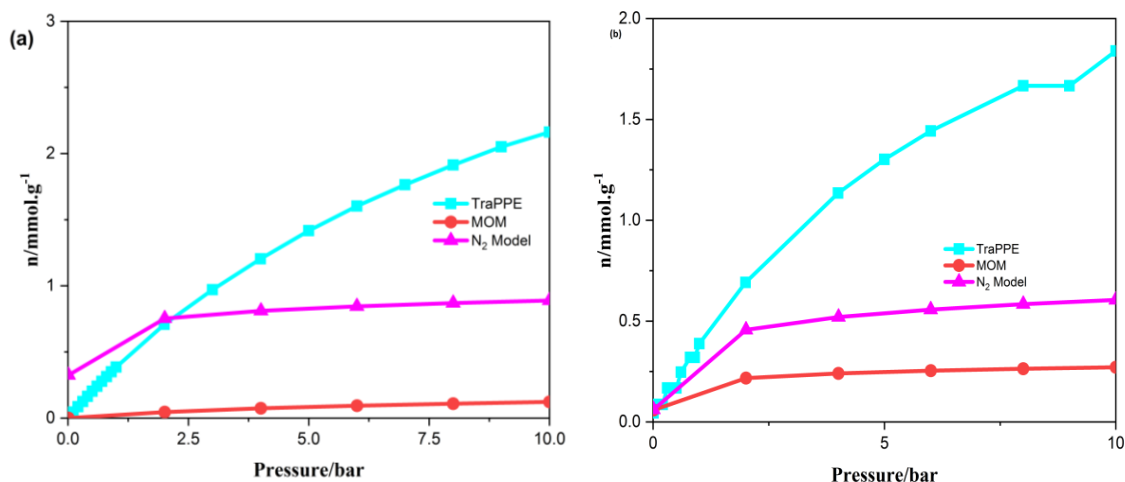
Fig. S4. Single component adsorption isotherm for simulated (closed) using general force field and experimental (open) N_2 by DFT-optimized dry structures FEFFIVE-Ni-pyr-TB (a) and ALFFIVE-Ni-pyr-TB (b) at 298K
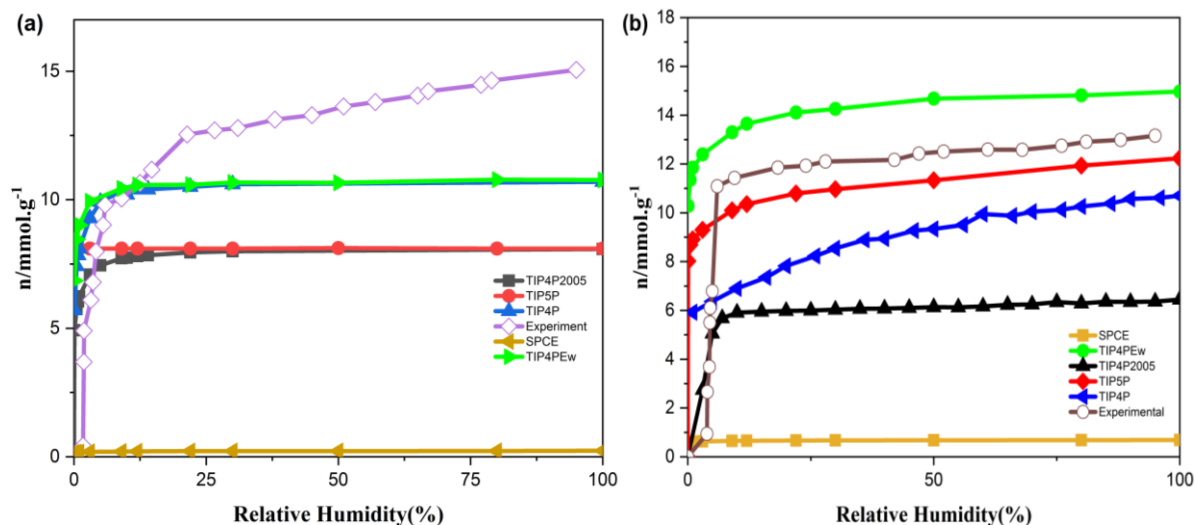
Fig. S5. Simulated single component adsorption isotherm for H_2O in DFT-optimized dry structures by generic force field, FEFFIVE-Ni-pyr-TB (a) and ALFFIVE-Ni-pyr-TB (b) at 298K

7.1. Comparison of the Enthalpy of adsorption
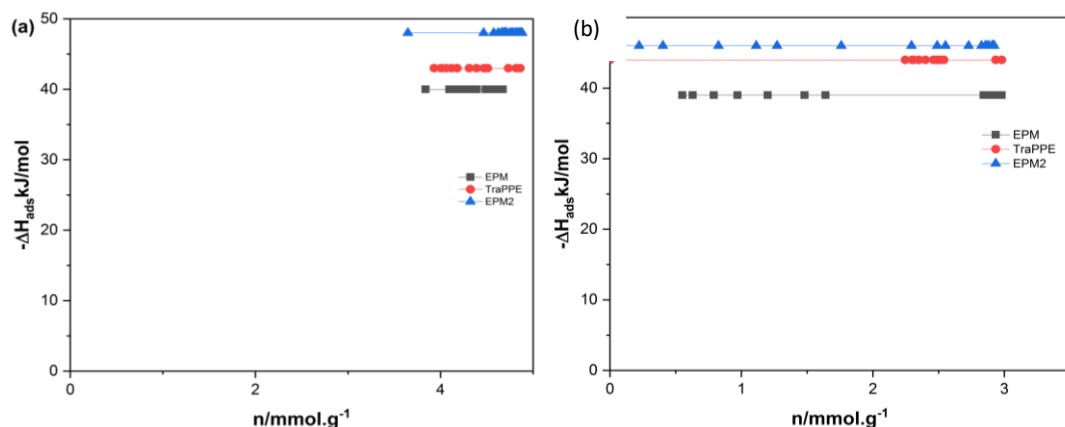
Fig. S6. Enthalpy of adsorption for CO_2 in DFT-optimized structuresat 298K: FEFFIVE-Ni-pyr-TB (a) and ALFFIVE-Ni-pyr-TB (b)
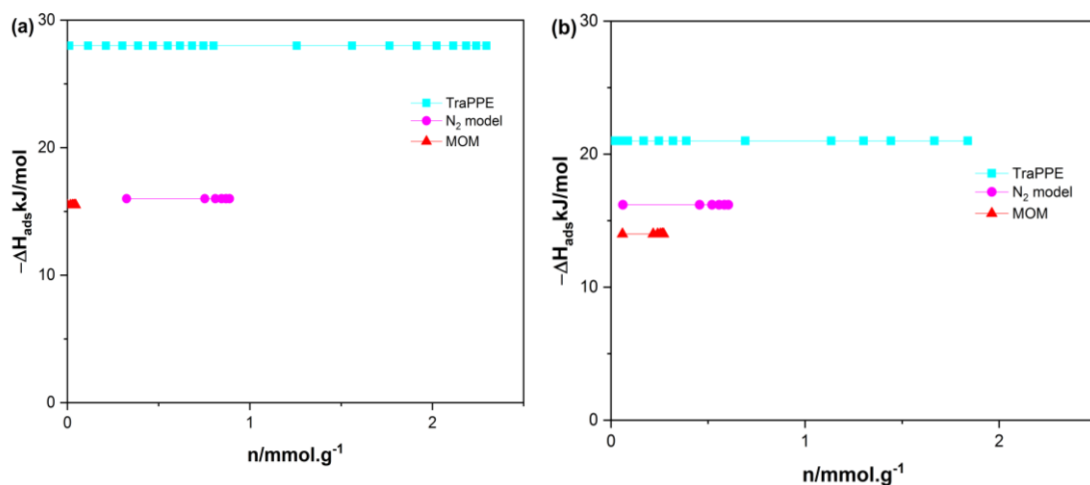
Fig. S7. Simulated enthalpy of adsorption using generic force field for N_2 in DFT-optimized structures at 298K: FEFFIVE-Ni-pyr-TB (a) and ALFFIVE-Ni-pyr-TB (b)
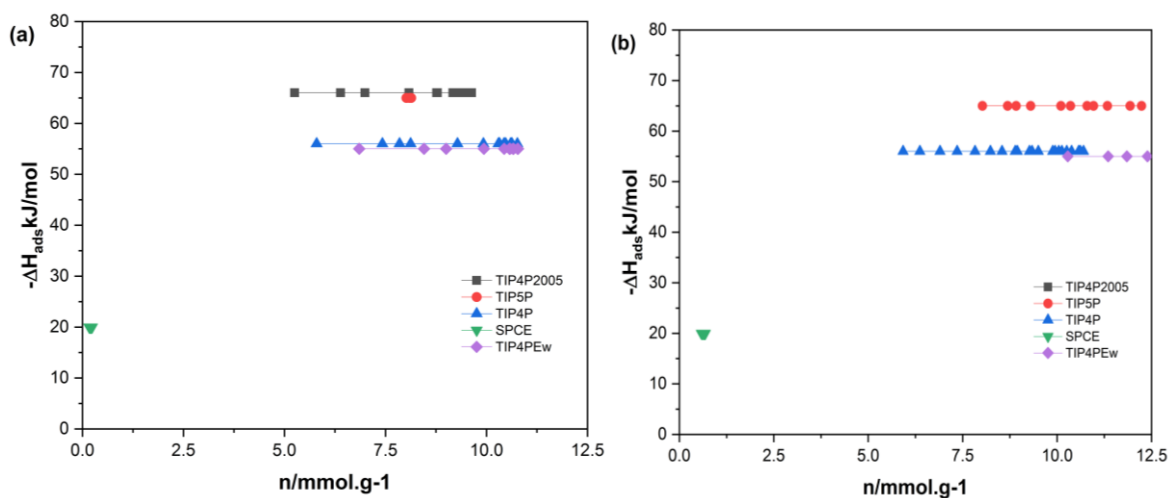
Fig. S8. Simulated enthalpy of adsorption using generic force field for H_2O in DFT-optimized structures at 298K: FEFFIVE-Ni-pyr-TB (a) and ALFFIVE-Ni-pyr-TB (b)

8. Single component adsorption Isotherm on wet structures, FE/ALFFIVE-Ni-pyr-SB
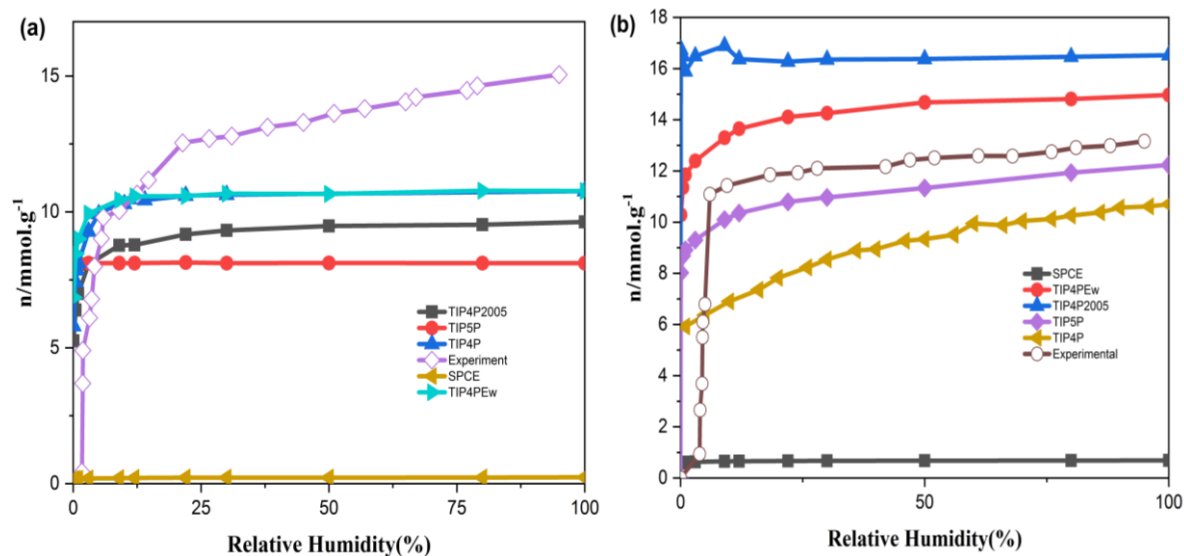
Fig. S9. Simulated (closed) using generic force field and experimental (open) single component adsorption isotherms for H_2O at 298K in DFT-optimized H_2O-loaded structure of FEFFIVE-Ni-pyr-SB (a) and ALFFIVE-Ni-pyr-SB (b).
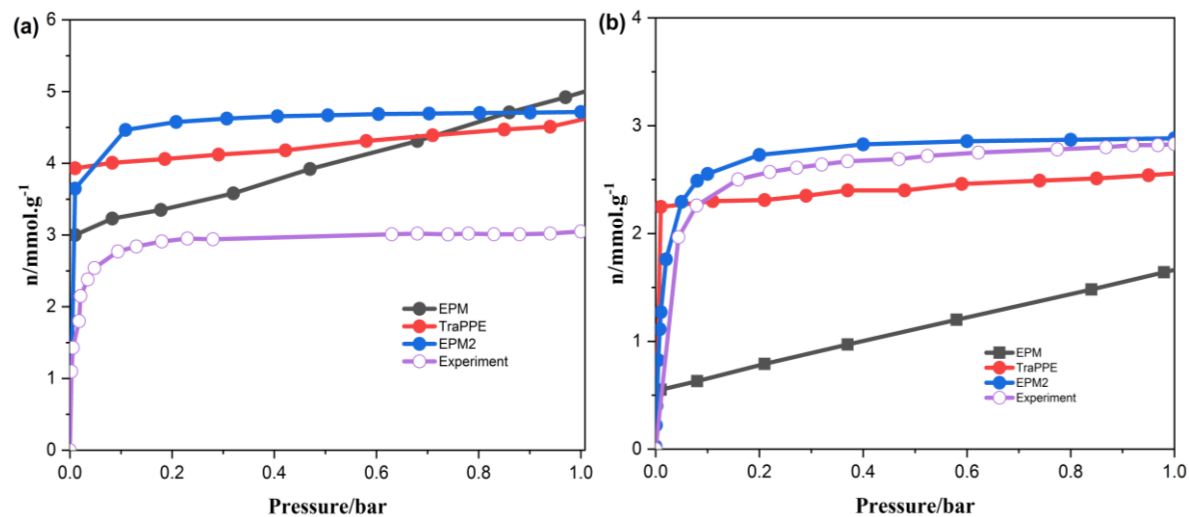
Fig. S10. Simulated (closed) using generic force field and experimental (open) single component adsorption isotherms for CO_2 at 298K in DFT-optimized H_2O-loaded structure of FEFFIVE-Ni-pyr-SB (a) and ALFFIVE-Ni-pyr-SB (b).
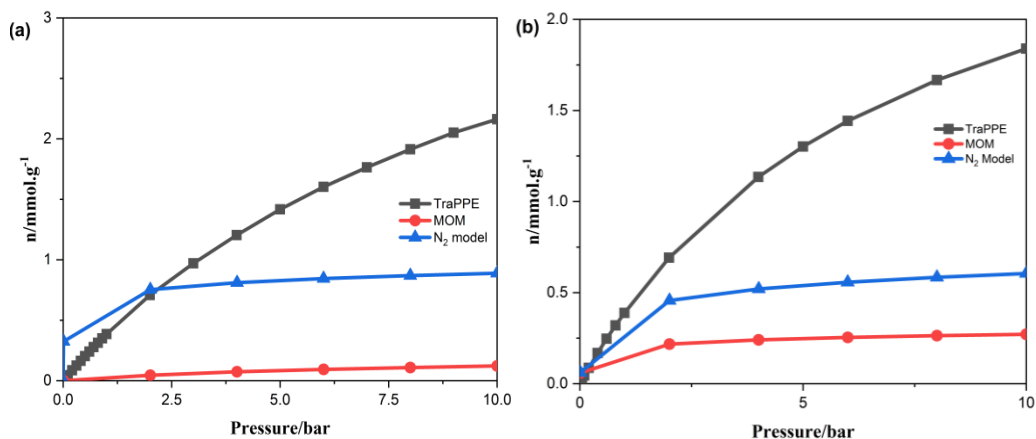
Fig. S11. Simulated (closed) using generic force field and experimental (open) single component adsorption isotherms for CO_2 at 298K in DFT-optimized H_2O-loaded structure of FEFFIVE-Ni-pyr-SB (a) and ALFFIVE-Ni-pyr-SB (b).
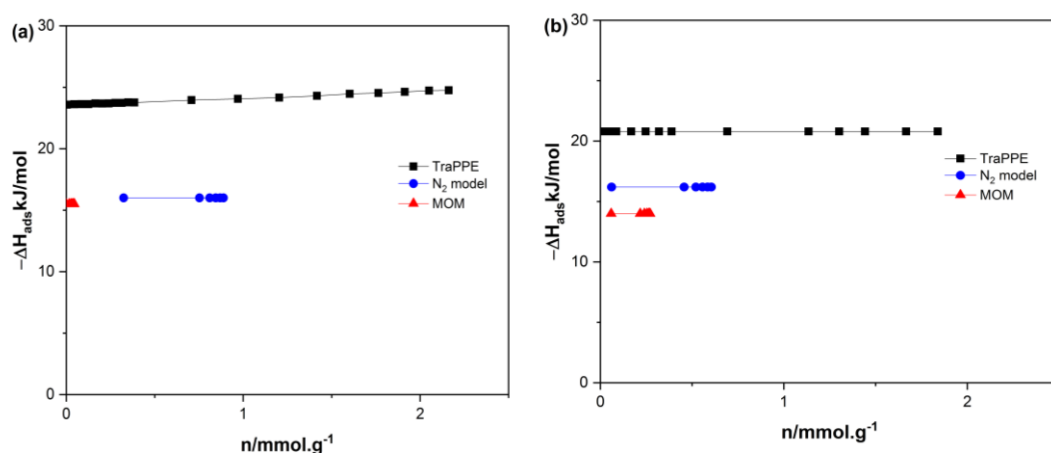
8.1 Comparison of the Enthalpy of adsorption
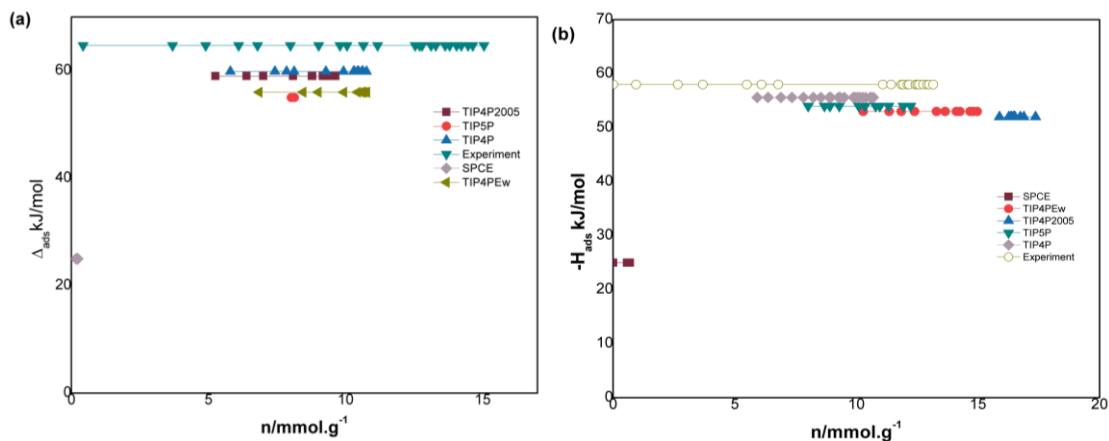
Fig. S12. Enthalpy of adsorption simulated (closed) using generic force field and experimental (open) for H_2O in DFT-optimized water loaded structures of FEFFIVE-Ni-pyr-SB (a) and ALFFIVE-Ni-pyr-SB (b) at 298K.
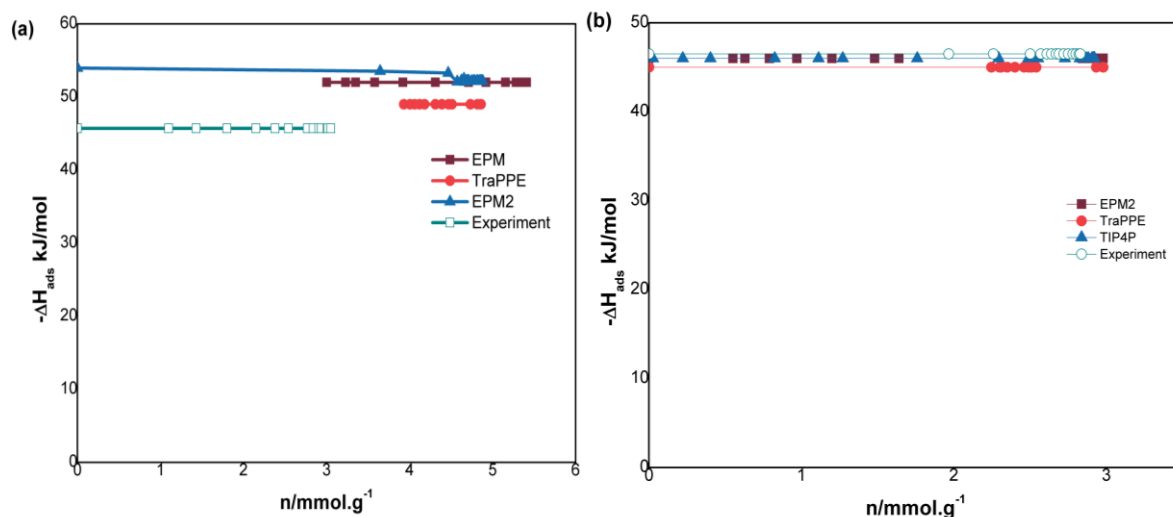
Fig. S13. Enthalpy of adsorption simulated (closed) using generic force field and experimental (open) for CO_2 in DFT-optimized water loaded structures of FEFFIVE-Ni-pyr-SB (a) and ALFFIVE-Ni-pyr-SB (b) at 298K.

Fig. S14. Enthalpy of adsorption simulated (closed) using generic force field and experimental (open) for N_2 in DFT-optimized water loaded structures of FEFFIVE-Ni-pyr-SB(a) and ALFFIVE-Ni-pyr-SB(b) at 298K.

8.2 Radial Distribution Functions calculated for single component adsorption using generic force filed in FEFFIVE-Ni-pyr-SB, after achieving local flexibility upon H_2O-loading.(TIP4P[30] model)

 (a) H_2O
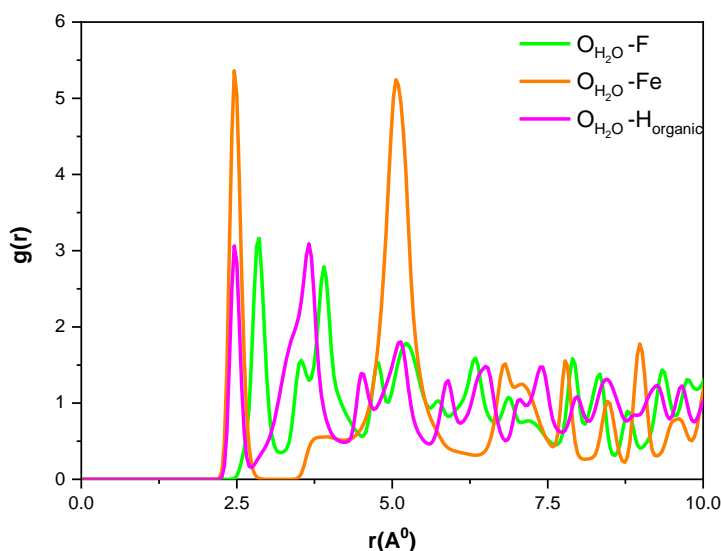
Fig. S15. Radial distribution functions (RDF) between H_2O and the atoms of the framework (Fluorine, F: green, Pyrazine hydrogen, H pyr: magenta, Pyrazine Carbon, Cpyr: black) extracted from the single component adsorption in FEFFIVE-Ni-pyr-SB at 1 bar and 298 K.
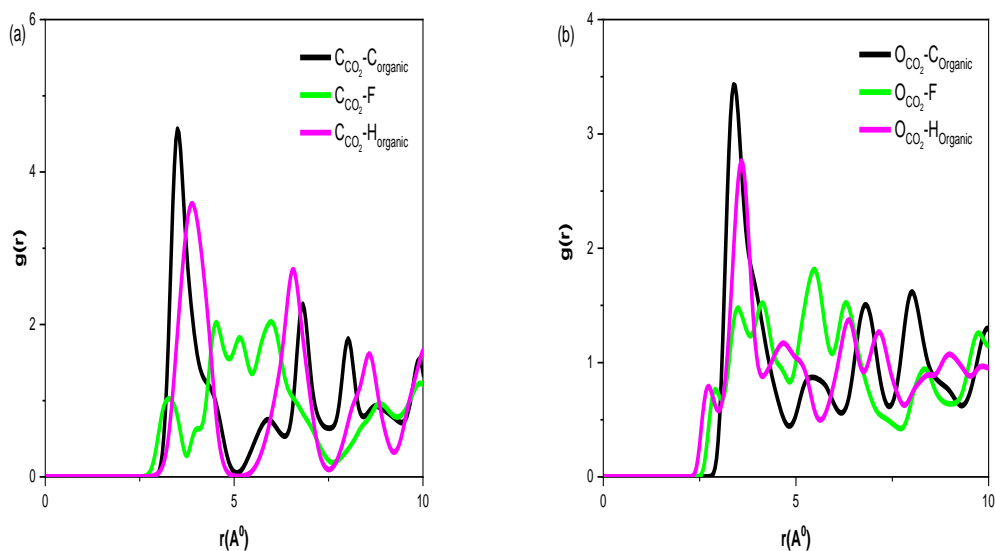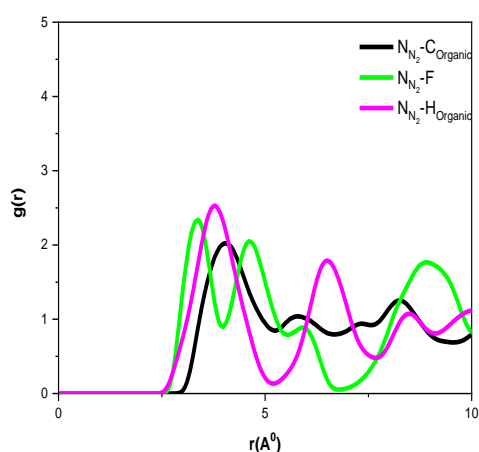
(b) CO₂

Fig. S16. Radial distribution functions (RDF) between CO_2 and the atoms of the framework (Fluorine, F: green, Pyrazine hydrogen, H_{pyr}: magenta, Pyrazine Carbon, C_{pyr}: black, Pyrazine nitrogen, N_{pyr}: Royal blue) extracted from the single component adsorption in FEFFIVE-Ni-pyr-SB at 1 bar and 298 K: Carbon of CO_2: C_{CO2} (a) and Oxygen of CO_2: O_{CO2} (b).

(c) N₂

Fig. S17. Radial distribution functions (RDF) between N_2 and the atoms of the framework (Fluorine, F: green, Pyrazine hydrogen, Hpyr: magenta, Pyrazine Carbon, Cpyr: black) extracted from the single component adsorption in FEFFIVE-Ni-pyr-SB at 1 bar and 298 K.

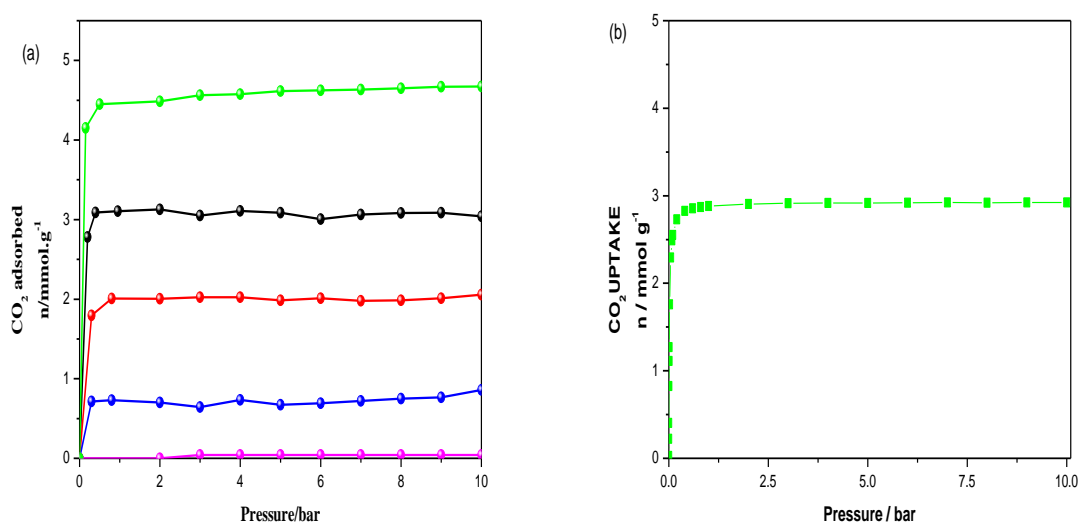## 9. Co-adsorption using generic force field – CO_2 adsorption in presence of H_2O in loaded structure based on TIP4P[29] model.

Fig. S18. Simulated co-adsorption isotherm for CO_2 in presence of various concentration of water (TIP4P), (a) FEFFIVE-Ni-pyr-SB and (b) ALFFIVE-Ni-pyr-SB. (RH = 0%, green; 4.871 %, black; 9.7427%, red ;14.6141%, blue; 19.4855%, violet, 24.0 %, pink)

9.1. Radial Distribution Functions calculated for single component adsorption of FEFFIVE-Ni-pyr-SB in humid condition.
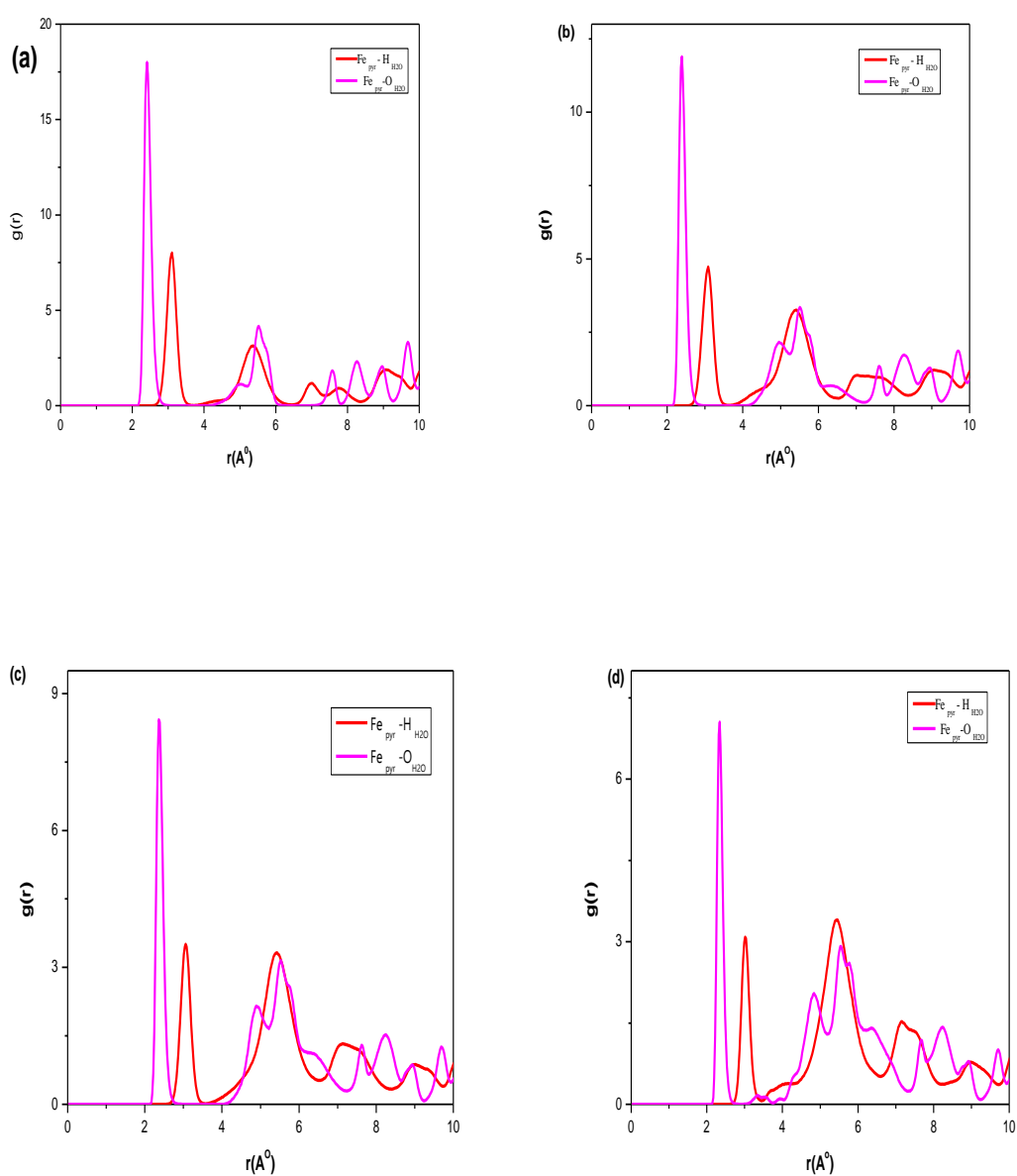
Fig. S19. Radial distribution functions (RDF) between guest molecules (H_2O) and the atoms of the framework in FEFFIVE-Ni-pyr-SB.(RH=4.871 %, (a); 9.7427 %,(b) ;14.6141%, (c); 19.4855%,(d))

10. Separation of CO_2/N_2 mixture in presence of humidity by utilizing generic force field.
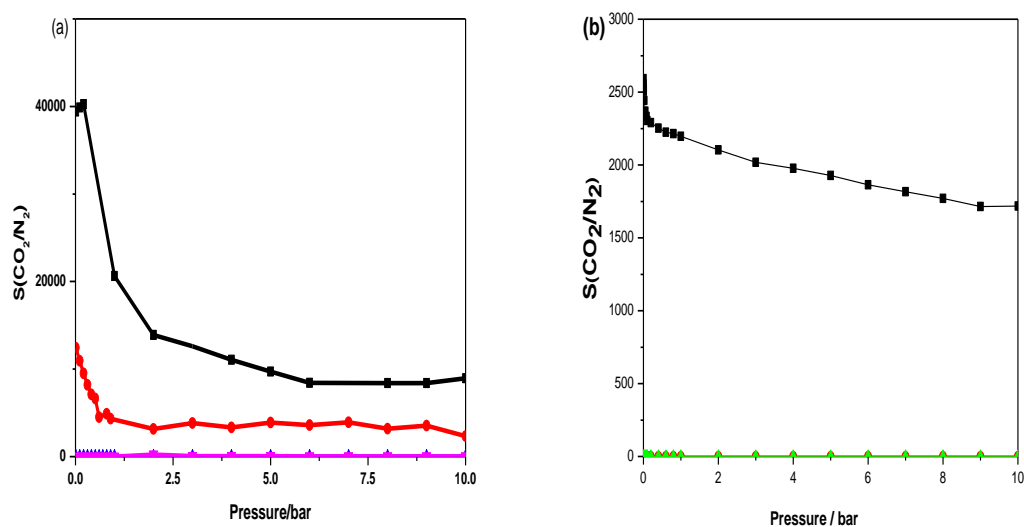
Fig. S20. Simulated selectivity's for CO_2/N_2 from their 15/85 molar ratio gas mixture in DFT-optimized H_2O-loaded structures utilizing generic force field(TIP4P), (a) FEFFIVE-Ni-pyr-SB, (b) ALFFIVE-Ni-pyr-SB (water loaded = 4.871 %, square; 9.7427%, circle; 14.6141%, up-triangle; 19.4855%, diamond).
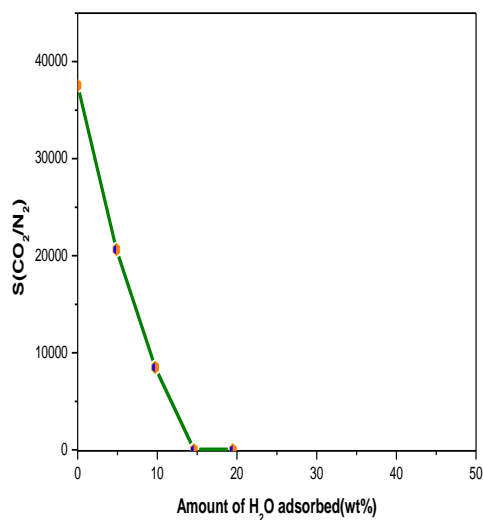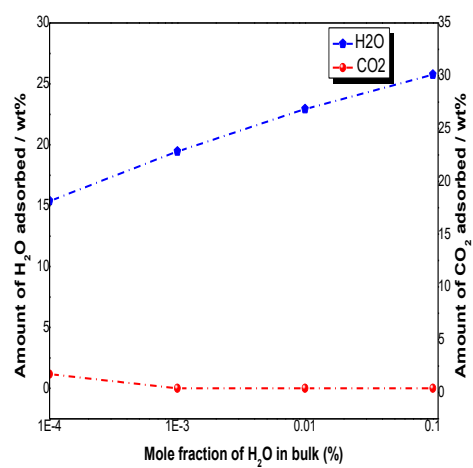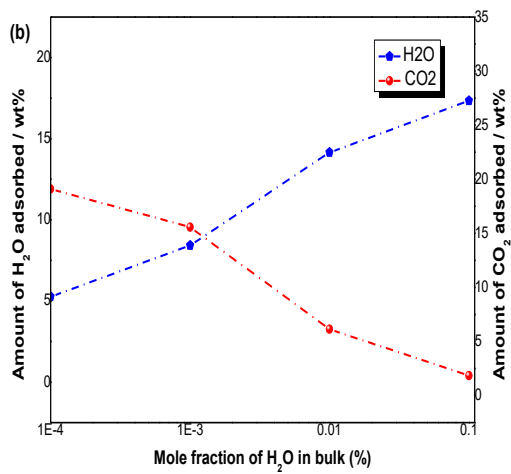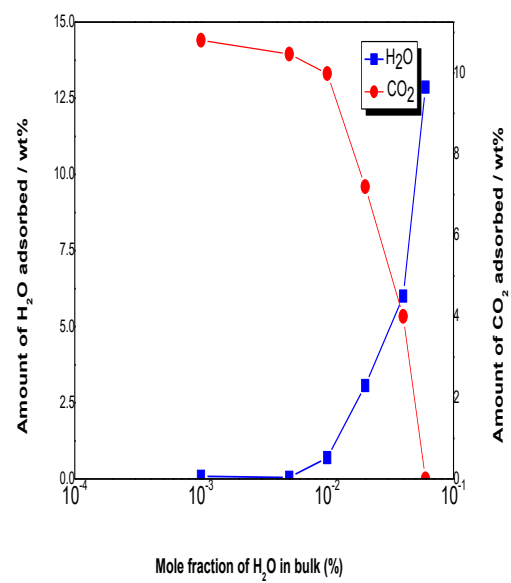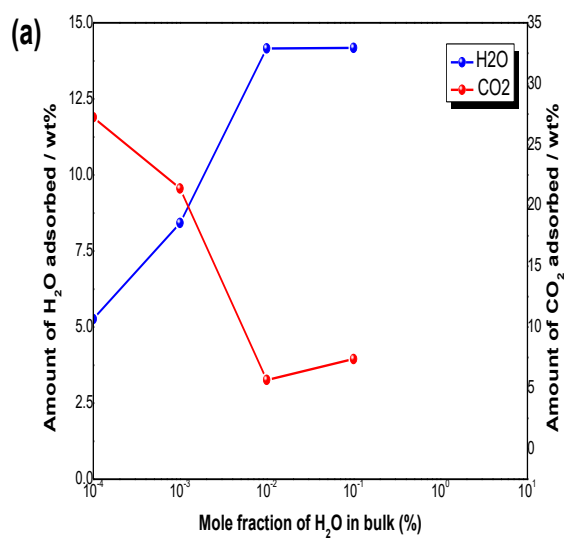

Fig. S21. Simulated selectivity for CO_2/N_2 from their 15/85 molar ratio gas mixture in DFT-optimized H_2O-loaded structure of FEFFIVE-Ni-pyr-SB utilizing generic force field, (water loaded = 0%,4.871%, 9.7427%, 14.6141%, 19.4855%).

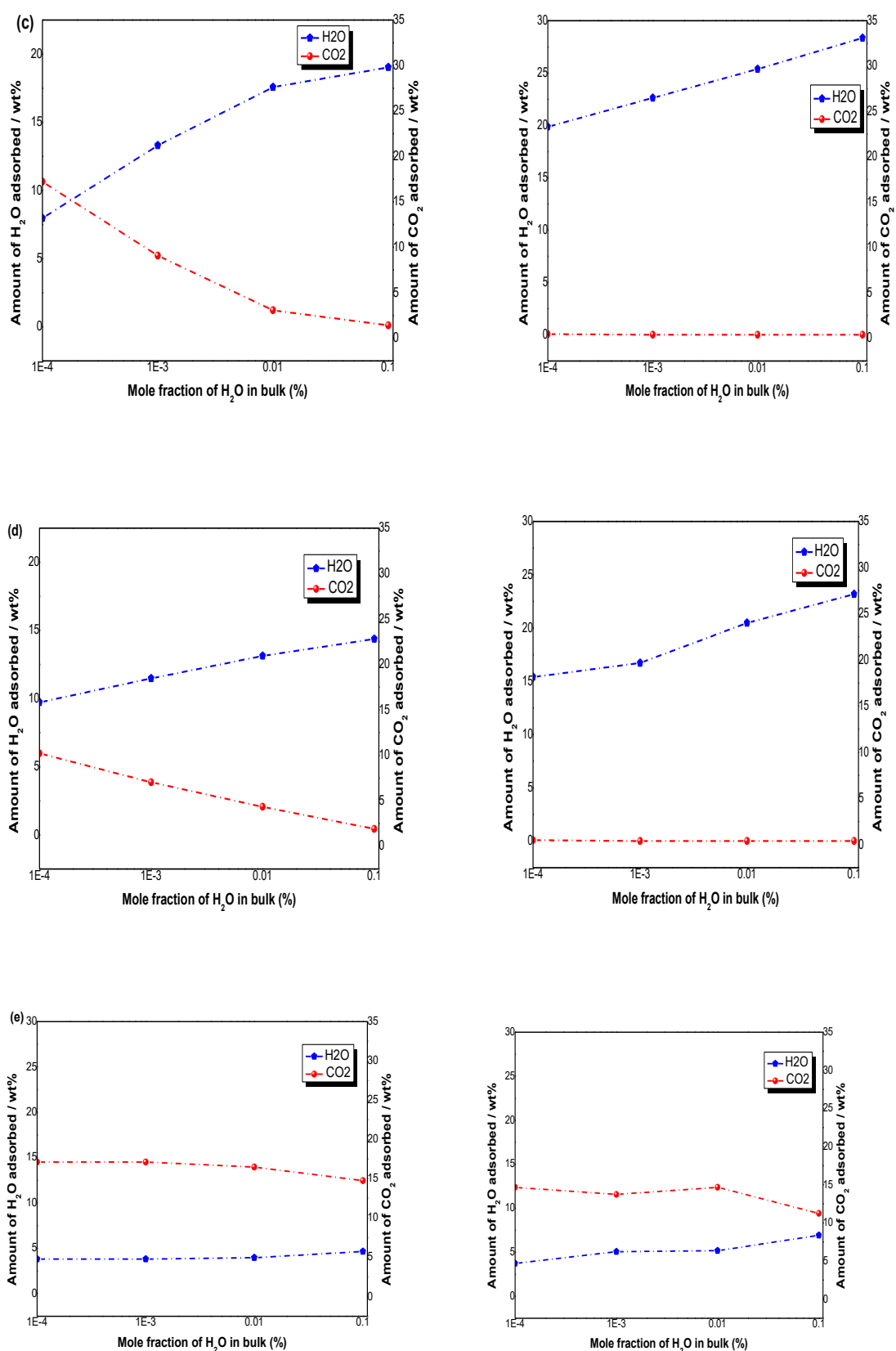## 11. Ternary adsorption involves H_2O, CO_2 and N_2 using Generic Force Field

Fig. S22. Simulated Ternary adsorption for H_2O, CO_2 and N_2 in FEFFIVE-Ni-pyr-SB (left) and ALFFIVE-Ni-pyr-SB (right) using generic forcefield as a function of H_2O mole fraction at

total pressure of 1.0 bar and temperature of 298 K. Uptake of H_2O (Left y-axis, closed blue squares) and CO_2 (Right y-axis, red closed circles) with adsorbate model: $H_2O/CO_2/N_2$ as (a) TIP4P/EPM2/TraPPE, (b) TIP4P2005/EPM2/TraPPE, (c) TIP4PEw/EPM2/TraPPE, (d) TIP5P/EPM2/TraPPE and (e) TIP4PEw/TraPPE/TraPPE.

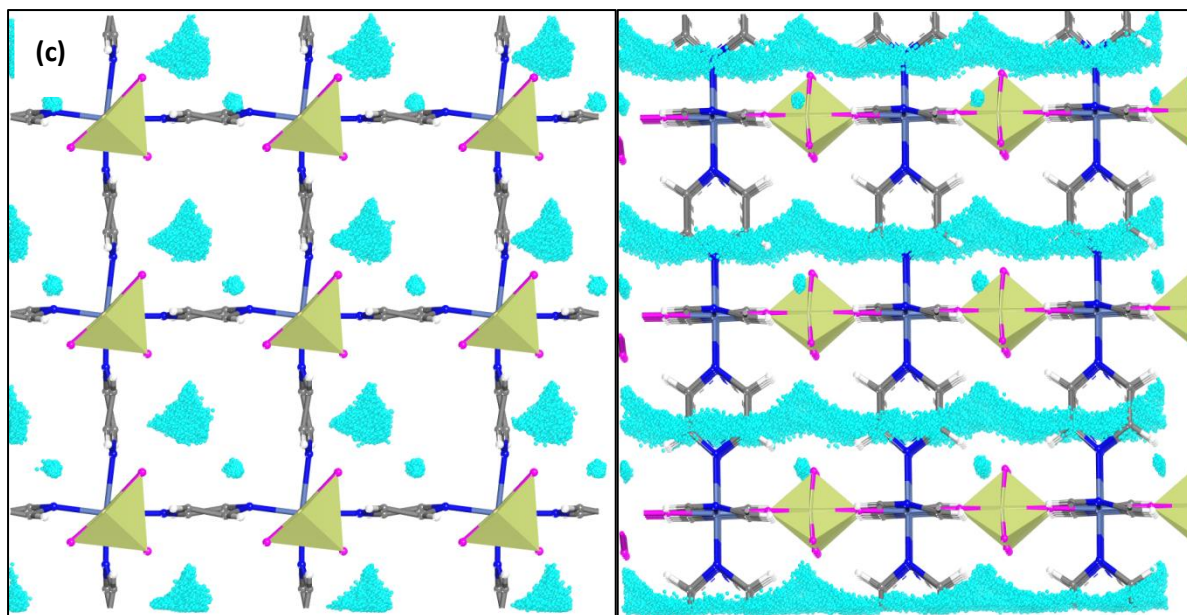## 12. Snapshot of loaded guest molecule in FEFFIVE-Ni-pyr-SB
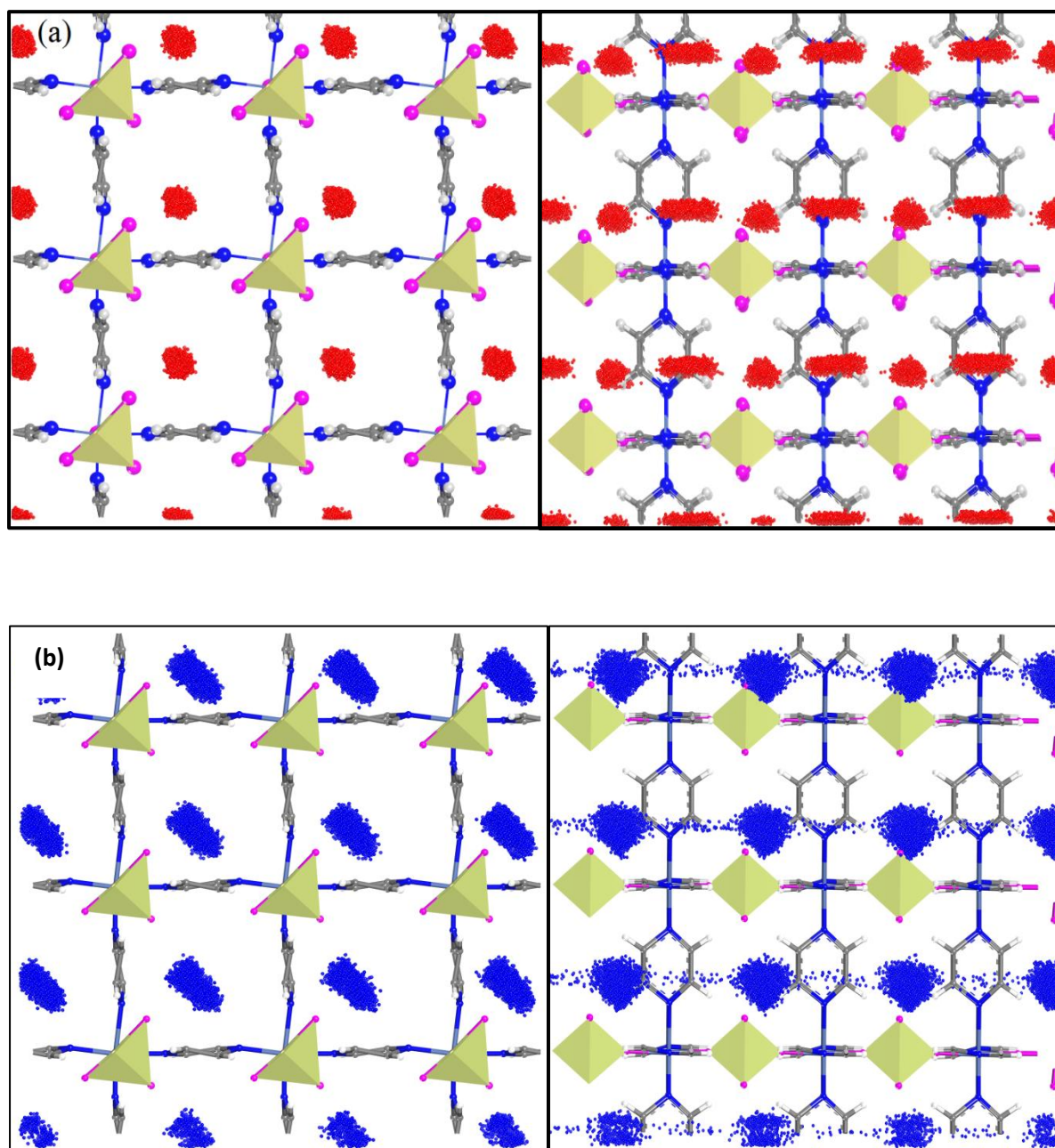
Fig. S23. Maps corresponding occupied positions of CO_2 (red), N_2 (blue) and H_2O, (with 19.5 wt %), (cyan) in 1000 equilibrated frames extracted from the GCMC simulations of FEFFIVE-Ni-pyr-SB utilizing generic force field.

13. GCMC Simulations – Using DFT-Derived Force field.

Interatomic potentials for describing the interaction between the adsorbate and CUS MOF framework in presence of humidity were derived by Quantum mechanically. Therefore, the extra potentials for Fe-H_2O are derived from DFT energy profile for the interaction between H_2O and Fe of MFFIVE-Ni-pyr-SB (M=Fe/Al).Where, the binding energy were calculated as follows,

$$E_{B.E} = E_{MOF+Guest} - E_{MOF} - E_{Guest} \qquad (4)$$

Where $E_{(MOF+Guest)}$ corresponds to the energy of optimized metal organic framework with loaded guest molecule and E_{MOF} and E_{Guest} indicates the energy of MOF and guest molecule individually. From the series of binding energy calculations by varying the Fe-adsorbate interatomic distance from 0.1 to 5 Å leads to the potential energy curve of Guest-host interaction in the system. The potential energy curve further evaluates for the derivation of new force field parameters to represent guest-host interaction. Grand canonical Monte Carlo (GCMC) was performed to determine the single component adsorption and adsorption enthalpy of guest molecule such as CO_2, N_2 and H_2O at 298K. Additionally binary adsorption, adsorption in presence of water and ternary were performed carefully.

13.1 Interatomic Potential parameters- DFT-Derived FF.

The interaction between guests molecules with MFFIVE-pyr-SB (M=Fe/Al) framework were explained through Vander Waals contribution, however two more analytical functions are employed to address Vander Waals term

  (a) The interaction between any guest molecules with all atoms of the frameworks except open metal site of Fe/Al using standard 12-6 Lennard Jones potential (LJ).(equation5)

$$U_{ij} = \underbrace{\sum_{\substack{i,j \\ i<j}} \frac{1}{4\pi\varepsilon_0} \frac{q_i q_j}{r_{ij}}}_{\textbf{Electrostatic term}} + \underbrace{4\varepsilon_{ij}\left[\left(\frac{\sigma_{ij}}{r_{ij}}\right)^{12} - \left(\frac{\sigma_{ij}}{r_{ij}}\right)^{6}\right]}_{\textbf{Lennard-Jones term}} \qquad (5)$$

Lennard-jones parameters are defined through Universal Field Parameters (UFF)[19] and DREIDING[20] generic fields for the inorganic and organic part of MOF framework, respectively. ε_{ij} and σ_{ij} indicates the interacting pair LJ parameter and the interaction parameters obtained through Lorentz-Berthelot mixing rules.(i.e., a geometric combining rule for the energy and an arithmetic one for the atomic size: $\varepsilon_{ij} = (\varepsilon_i \varepsilon_j)^{1/2}$ and $\sigma_{ij} = (\sigma_i + \sigma_j)/2$). The second term is the Columbic contribution between point charges q_i and q_j separated by a distance r_{ij}.)

  (b) The interaction between open metal site, Al/Fe, and guest molecule through Buckingham analytical function[36].(equation 6)

$$U_{ij} = \underbrace{\sum_{\substack{i,j \\ i<j}} \frac{1}{4\pi\varepsilon_0} \frac{q_i q_j}{r_{ij}}}_{\textbf{Electrostatic term}} + \underbrace{\left[A_{ij}e^{-B_{ij}r_{ij}} - S_g \frac{C_{ij}}{r_{ij}^6}\right]}_{\textbf{Buckingham term}} \qquad (6)$$

A, B and C are the conventional Buckingham parameters for repulsive and attractive contribution respectively and Sg indicates the global scaling factor for the dispersion energies. The DFT derived energy profile represented in Fig.S18 and S19 detailed as below.

Table S9: Buckingham parameters associated with the Fe/Al (III)-CUS-MOF with Adsorbates.

Adsorbates	Buckingham Parameters		
	A(kJ/mol)	B(A^0) $^{-1}$	C(kJ mol^{-1} $A^{0\,6}$)
Fe-Oe	7.06×10^8	10.19	558.556
Fe-C_CO$_2$	3.34×10^6	2.57	192.06×10^3
Fe-O_CO$_2$	1.11×10^7	2.66	114.41×10^4
Fe- N$_2$	7.58×10^4	3.67	1000
Al-Oe	8.87×10^5	3.63	5774
Al-C_CO$_2$	9.69×10^6	8.5	273.69×10^3
Al-O_CO$_2$	9.62×10^6	10.3	739.13×10^2
Al- N$_2$	9.68×10^5	8.79	820

13.1. Pathway of gases interaction towards framework of FEFFIVE-Ni-pyr-SB and ALFFIVE-Ni-pyr-SB
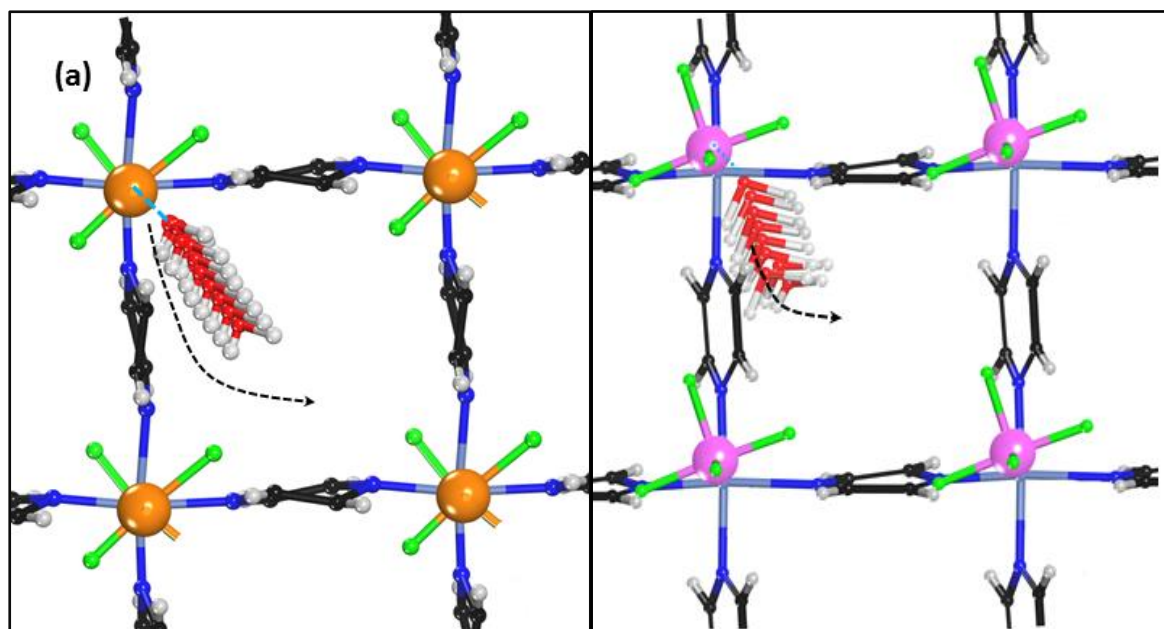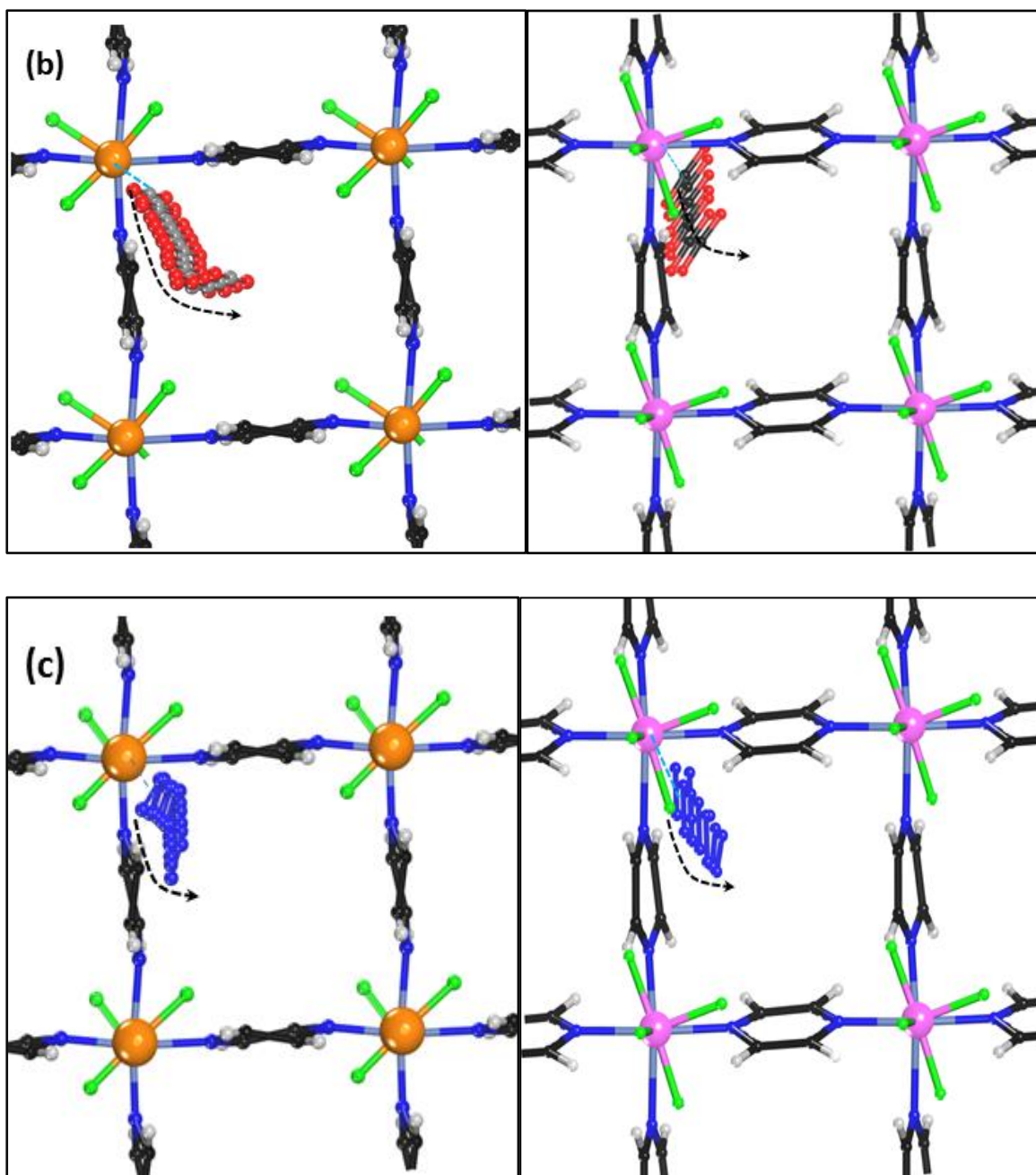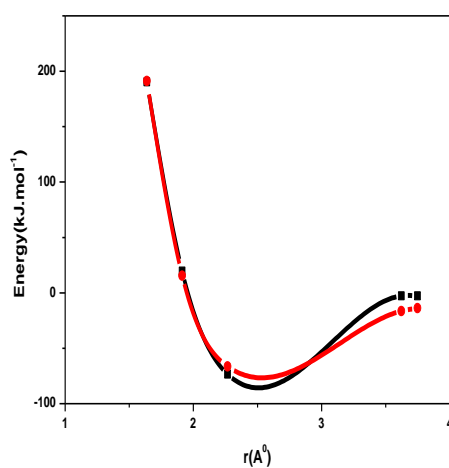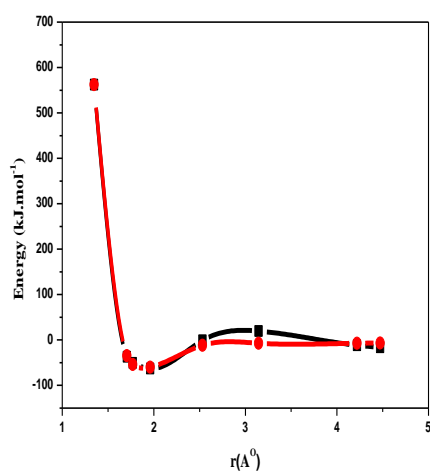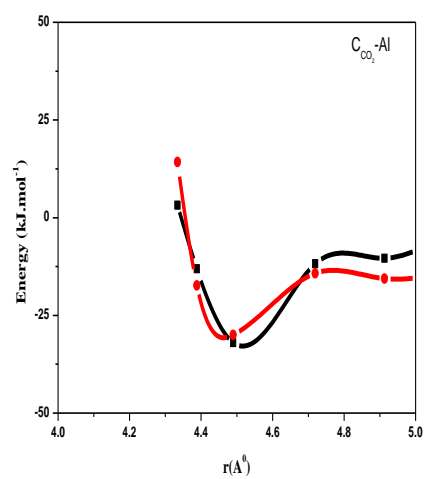
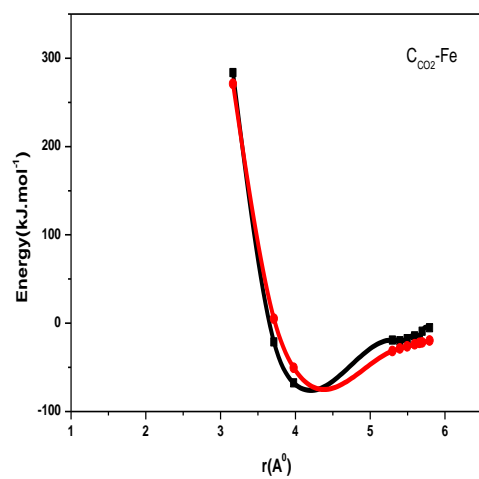**Fig. S24.** The systematic energetic pathway of interaction of guest molecule to the framework of FEFFIVE-Ni-pyr-SB (left) and ALFFIVE-Ni-pyr-SB (right) towards the H_2O (a), CO_2 (b) and N_2 (c) guest molecule

13.2. Force field parameterization for MFFIVE-Ni-pyr-SB (M=FE/AL) frame work *vs* guest interaction profile.

(a) H_2O interaction potential graph

(b) CO₂ interaction potential graph
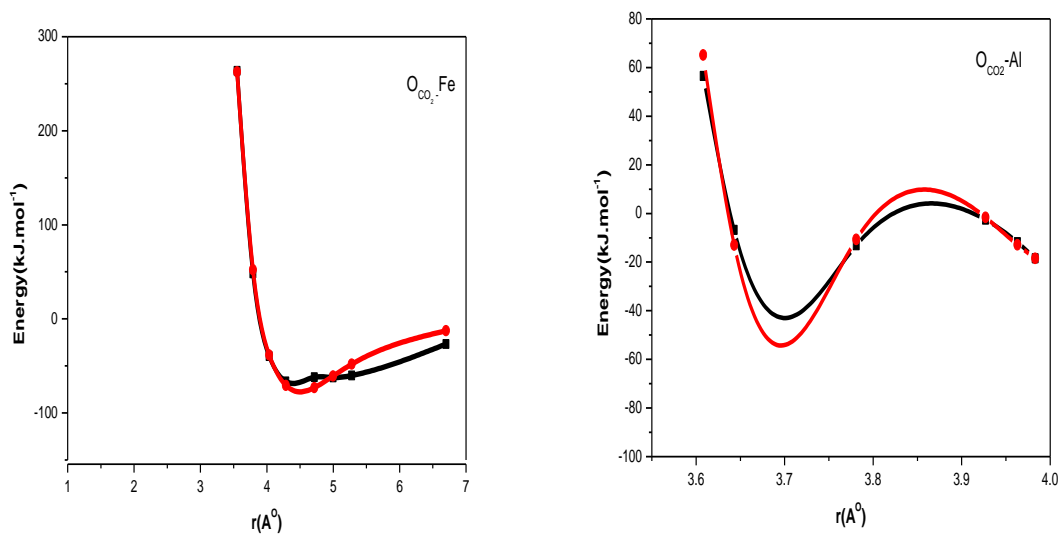
(c) N₂ interaction potential graph
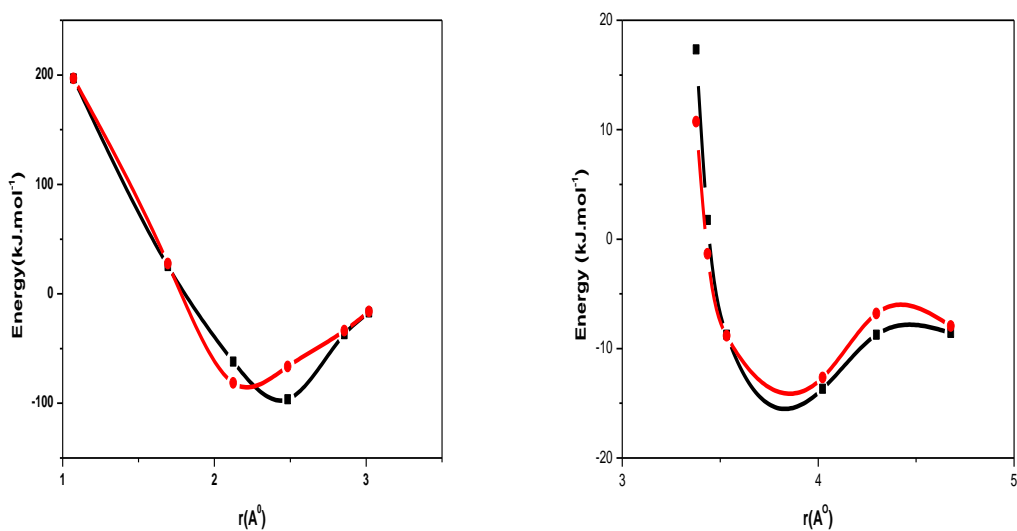
Fig. S25. Comparison of DFT-Derived FF fitted curve (red circles) on the DFT interaction energy profile (black squares) for FEFFIVE-Ni-pyr-SB (left) and ALFFIVE-Ni-pyr-SB (right) towards the H_2O (a), CO_2 (b) and N_2 (c) guest molecule.

14. Comparison of Isotherms (Simulated by DFT-derived FF *vs* Experimental)
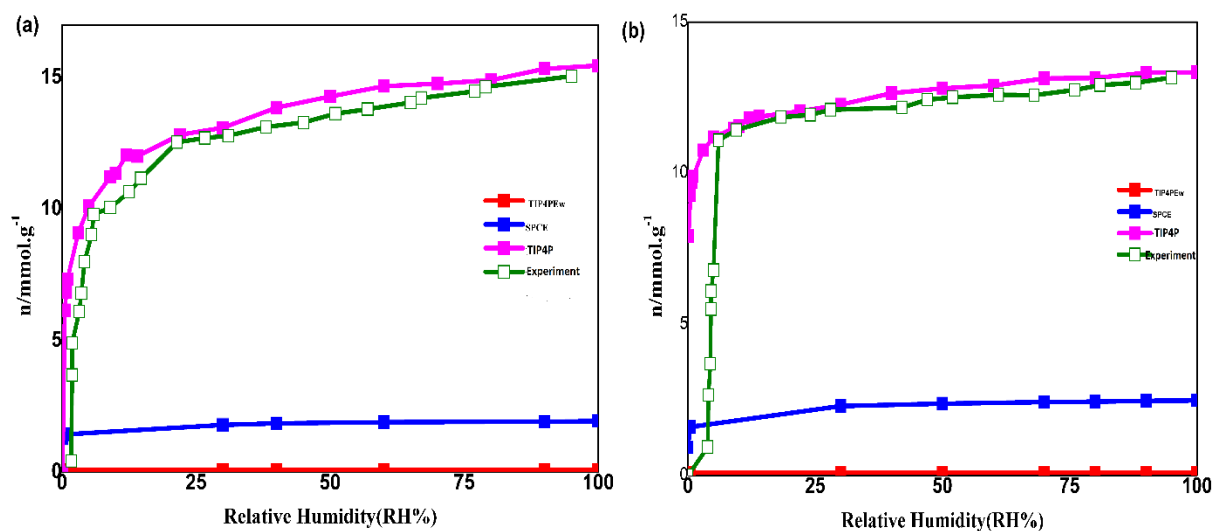
Fig. S26. Simulated DFT-derived FF (full symbol) and experimental (open symbol) single component adsorption isotherm for H_2O in FEFFIVE-Ni-pyr-SB (a) and ALFFIVE-Ni-pyr-SB (b) at 298K

CO_2 –EPM2 MODEL
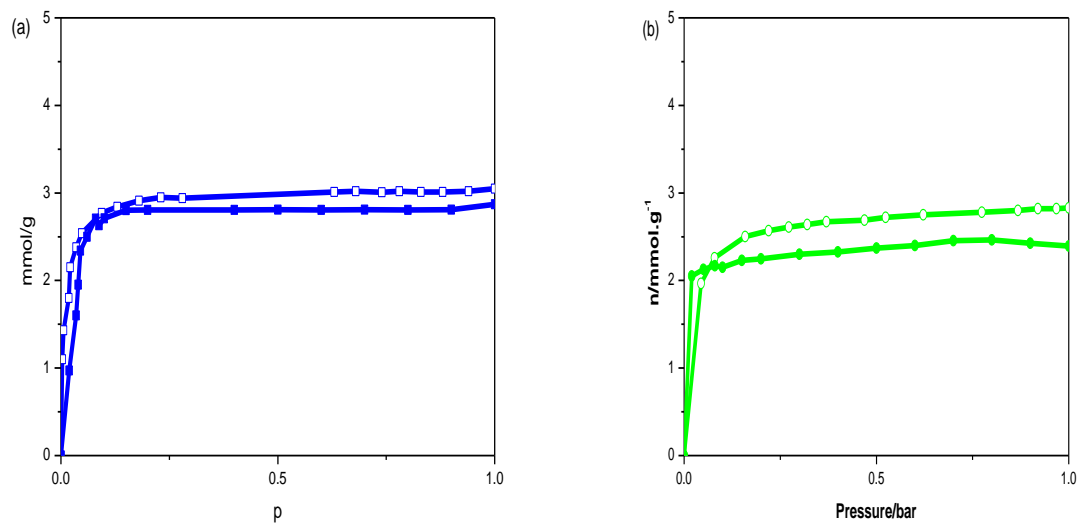
N_2 –TraPPE MODEL
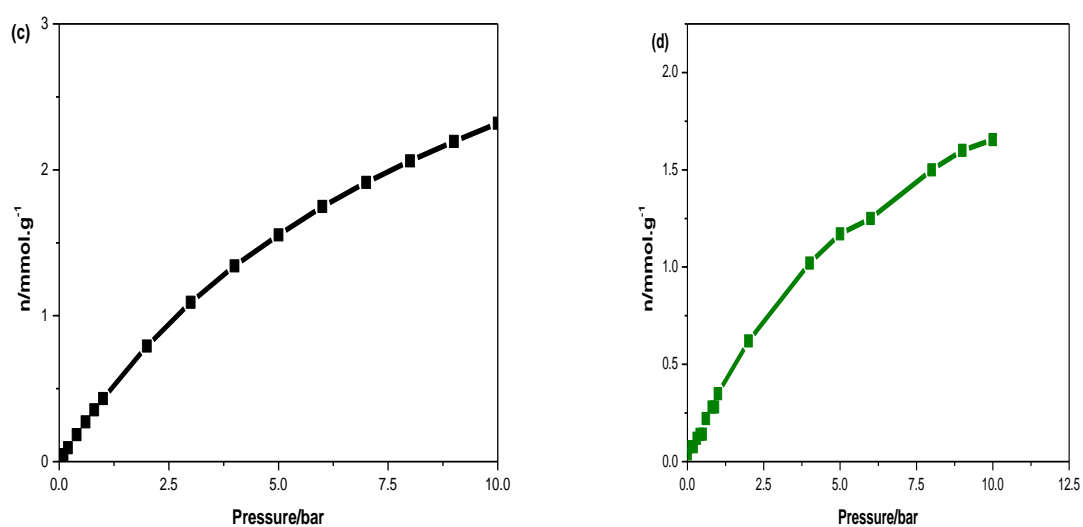
Fig. S27. Simulated (full symbol) by DFT-Derived FF and experimental (open symbol) single component adsorption isotherm for CO_2, N_2 in FEFFIVE-Ni-pyr-SB (left) and ALFFIVE-Ni-pyr-SB (right) at 298K

15. Enthalpy of Adsorption
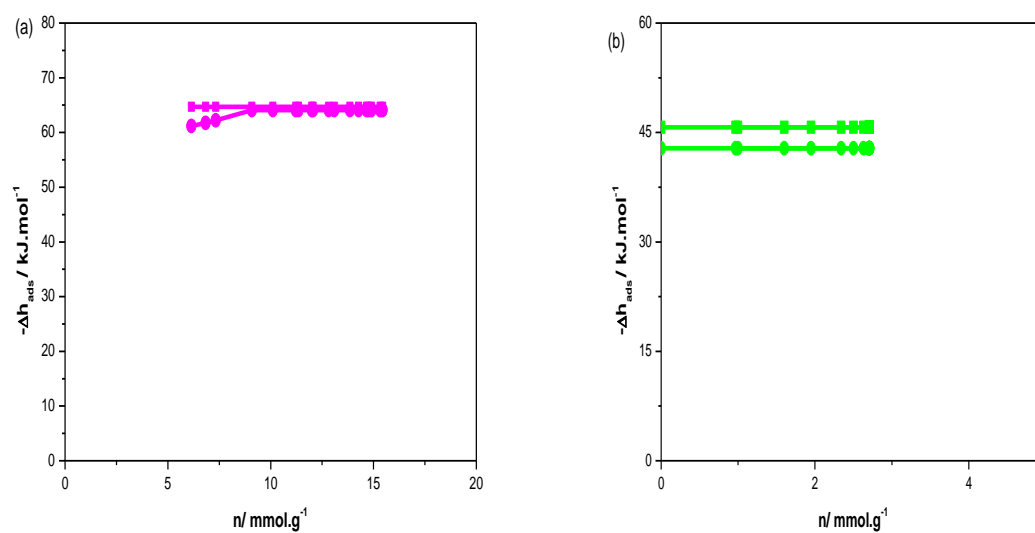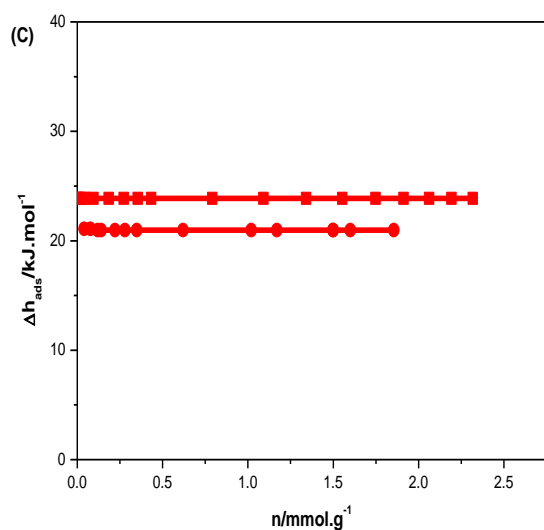
Fig. S28. Simulated enthalpy of adsorption with DFT-Derived FF for H_2O (a) CO_2 (b) and N_2 (c) in FEFFIVE-Ni-pyr-SB (square) and ALFFIVE-Ni-pyr-SB (sphere) at 298K

16. Co-adsorption – CO_2 adsorption in wet structures using newly DFT-Derived FF.
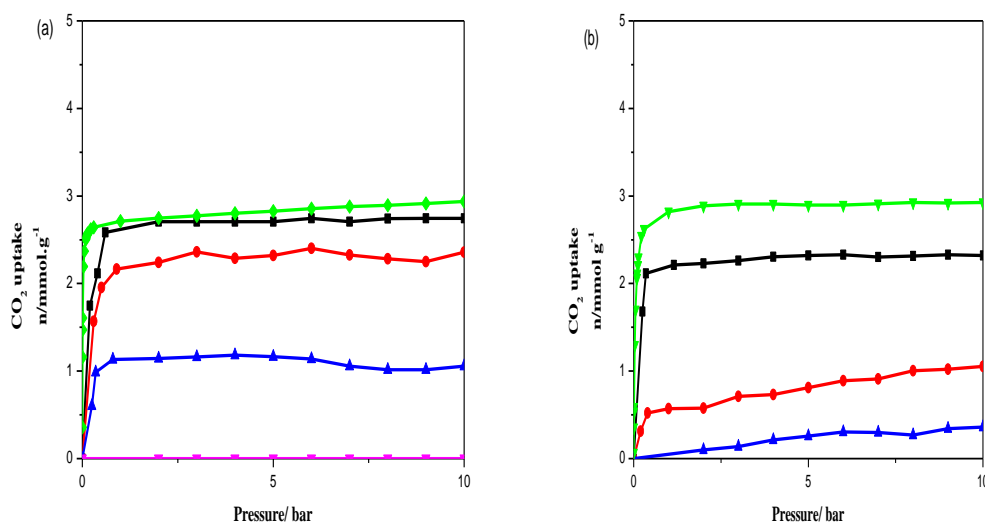
Fig. S29 : Simulated co-adsorption isotherm for CO_2 in presence of various concentration of water, (a) FEFFIVE-Ni-pyr-SB and (b) ALFFIVE-Ni-pyr-SB using newly DFT-derived FF (RH = 0%, green; 4.871%, black; 9.7427%, red; 14.6141%, blue; 19.4855%, violet, 24.343%, pink)
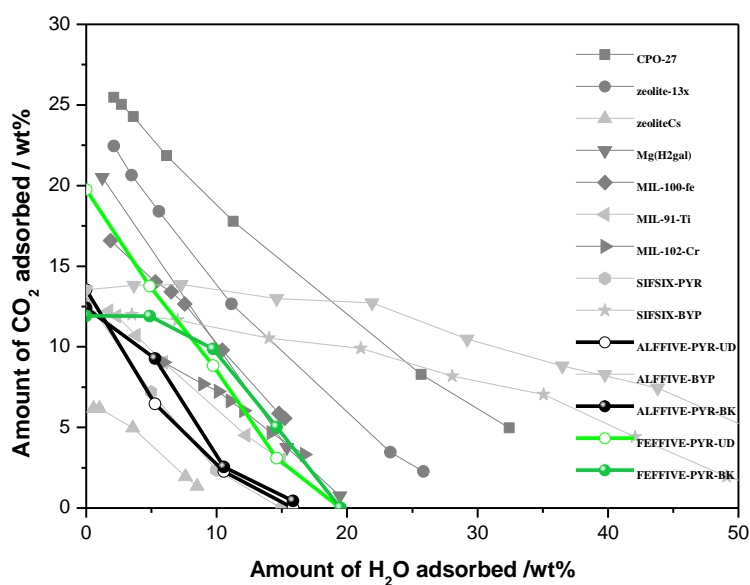
Fig. S30. Evolution of CO_2 uptake as a function of the amount of pre-adsorbed water on a series of MOFs.[14,37] (Green colour specify the present work)

16.1. Radial Distribution Functions calculated for single component adsorption using DFT-derived FF.
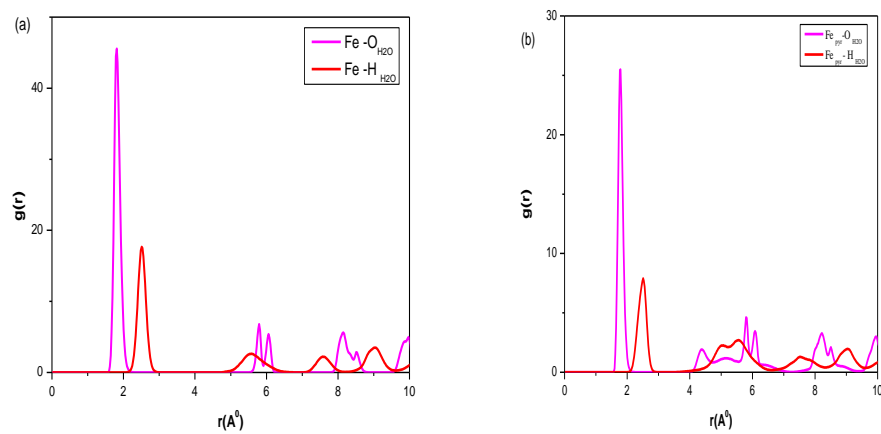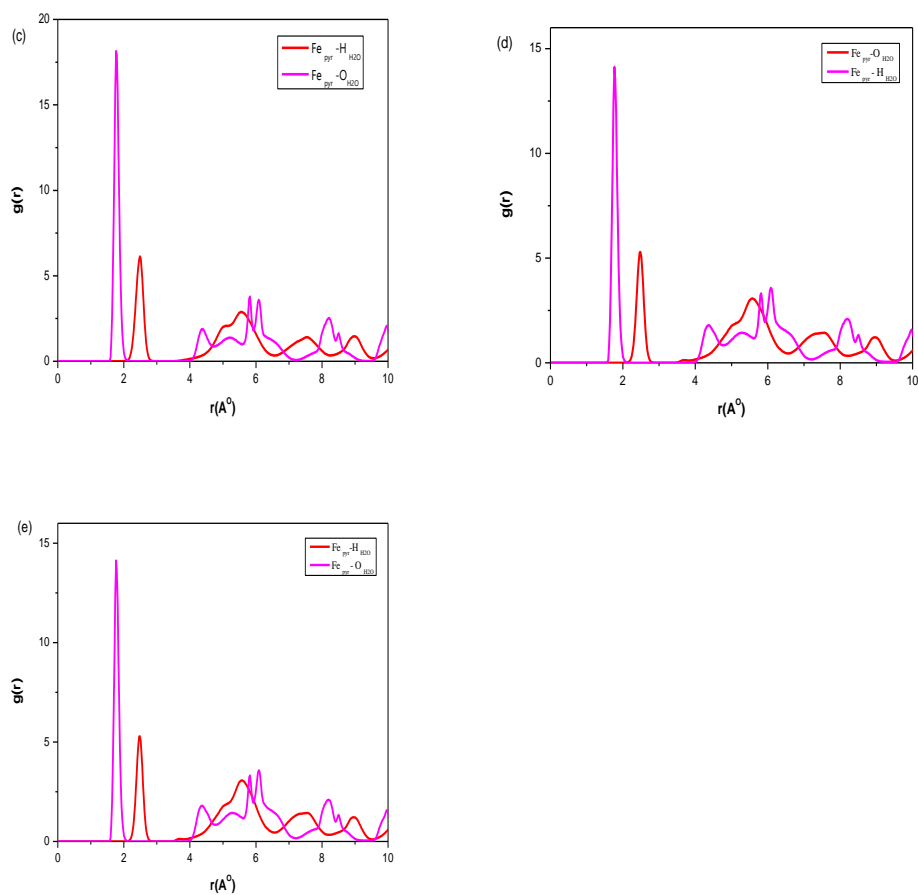
Fig. S31. Radial distribution functions (RDF) between guest molecules (H_2O) and the atoms of the framework in FEFFIVE-Ni-pyr-SB with DFT-derived FF. (RH=4.871 %, (a); 9.7427%, (b); 14.6141%, (c); 19.4855%, (d); 24.343%, (e)).

17. Separation of CO_2/N_2 mixture in presence of humidity using DFT-derived FF.
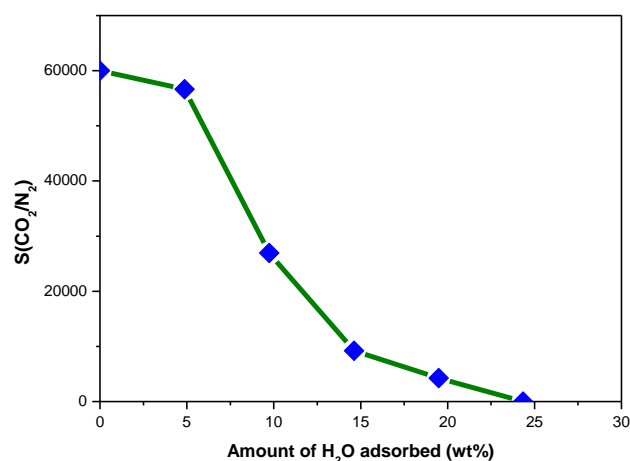
Fig. S32. Simulated selectivity's for CO_2/N_2 with 15/85 molar ratio gas mixture in FEFFIVE-Ni-pyr-SB using newly DFT-Derived FF.

18. Ternary adsorption utilizing DFT-derived FF involvesH_2O, CO_2 and N_2
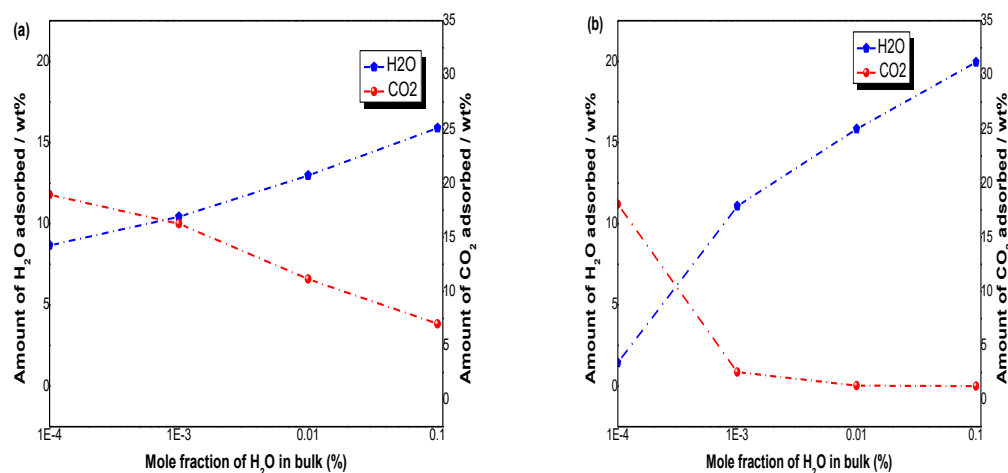
Fig. S33. Ternary co-adsorption for the flue gas composition, H_2O, CO_2 and N_2, in FEFFIVE-Ni-pyr-SB (a) and ALFFIVE-Ni-pyr-SB (b) by using newly DFT-derived FF. Uptake of H_2O (Left y-axis, closed blue squares) and CO_2 (Right y-axis, red closed circles) as a function of H_2O mole fraction at total pressure of 1.0 bar and temperature of 298 K.

18.1 Comparison of Radial Distribution Function of adsorbate interaction.
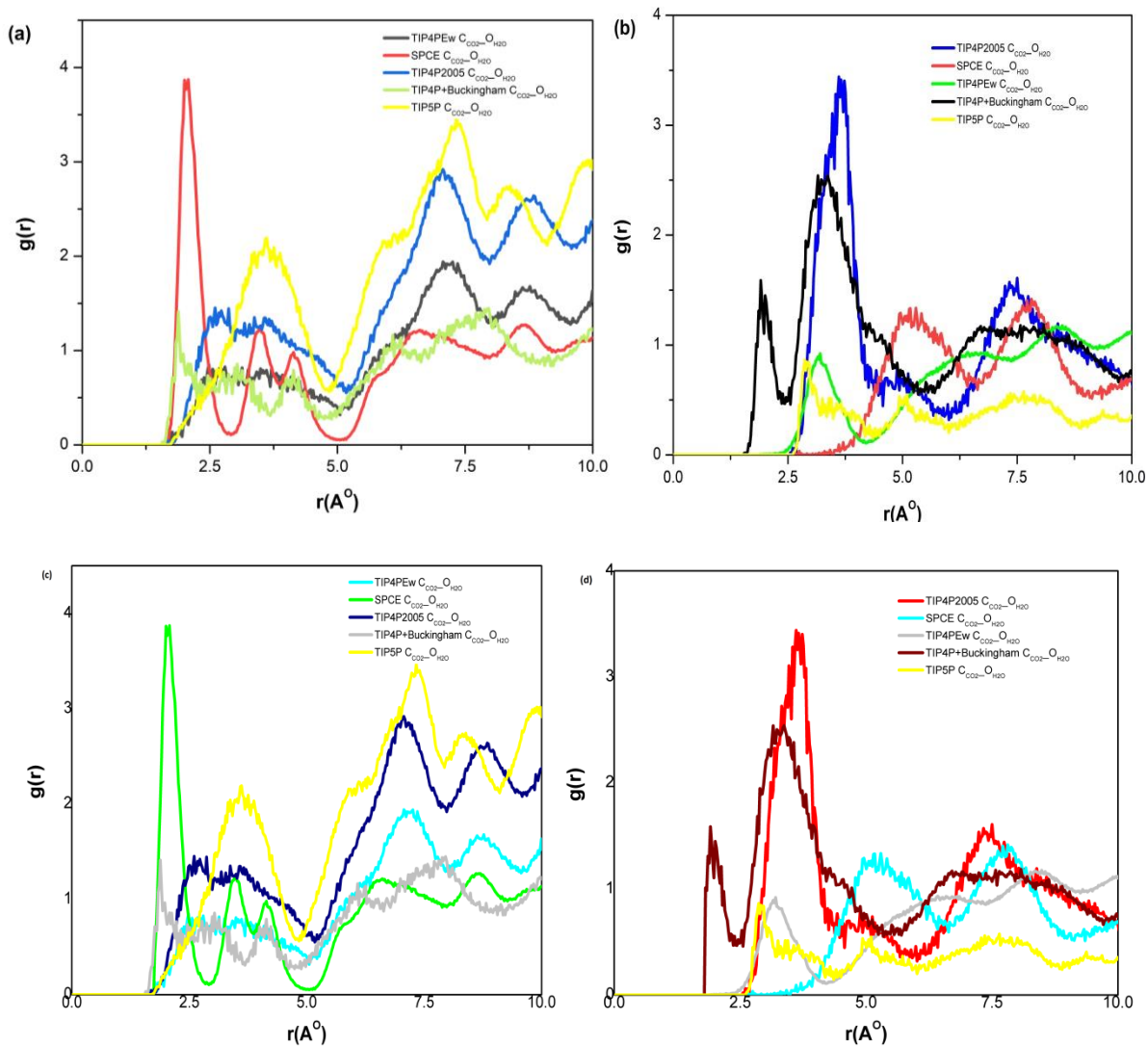
Fig. S34: Radial distribution functions (RDF) between guest molecules (H_2O) having different models and CO_2 model for FEFFIVE-Ni-pyr (left) and ALFFIVE-Ni-pyr (right) at 1bar (a, b) and 10 bar (c, d).
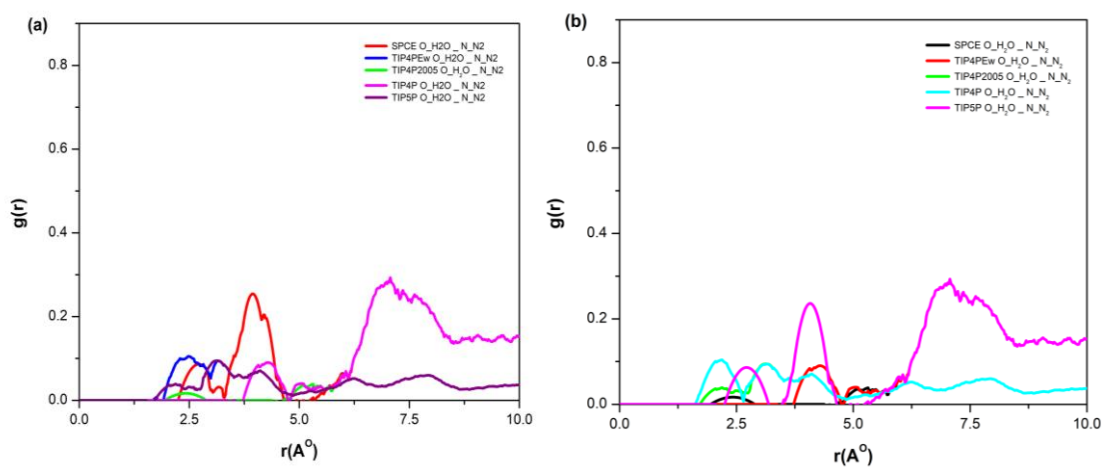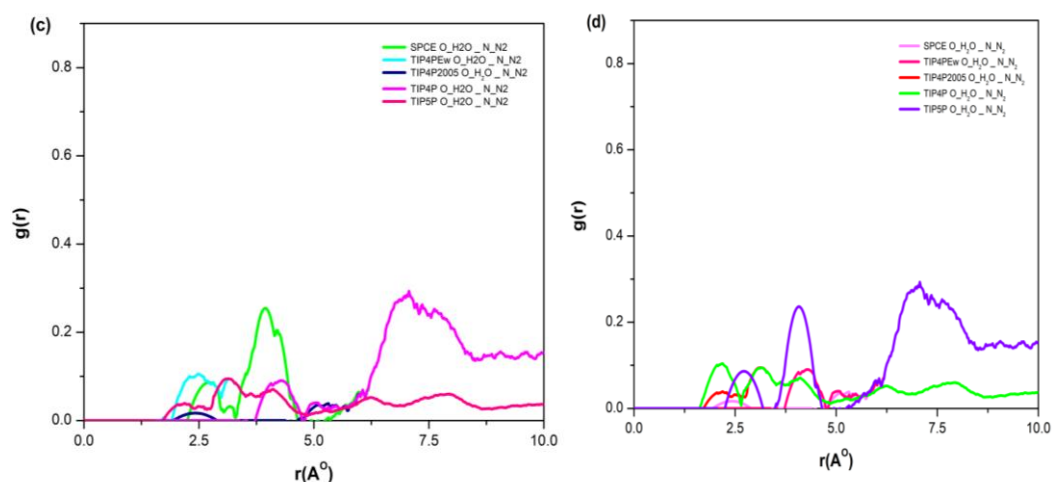
Fig. S35: Radial distribution functions (RDF) between guest molecules (H_2O) having different models and N_2 (TraPPE) model for FEFFIVE-Ni-pyr (left) and ALFFIVE-Ni-pyr (right) at 1bar (a, b) and 10 bar (c, d).

Table S10. Comparison of CO_2 / N_2 selectivity for a series of MOFs and conventional adsorbents in dry conditions at 1 bar and 298-303K.

Name	Mixture	%CO_2 in mixture	Selectivity	Calculation method	Ref
eea-MOF-4	CO_2/N_2	10	18	IAST[38]	[38]
rtl-MOF-2	CO_2/N_2	10	38	IAST[38]	[38]
SIFSIX-2Cu-i	CO_2/N_2	10	72	Measurement[39]	[39]
Eufcu-MOF	CO_2/N_2	10	82	IAST[40]	[40]
SIFSIX-3-Cu	CO_2/N_2	10	15000	IAST[41]	[41]
$Zn_4(pydc)_4(DMF)_2 \cdot 3DMF$	CO_2/N_2	15	42	IAST[42]	[42]
UiO-66 (Zr) BTEC	CO_2/N_2	15	56	Measurement[43]	[43]
Ni/DOBDC	CO_2/N_2	15	38	Measurement[44]	[44]
CAU-13(Al)	CO_2/N_2	15	22 *	IAST	[45]
CPO-27(Ni)	CO_2/N_2	15	13 *	IAST	[45]
CuBTC	CO_2/N_2	15	19 *	IAST	[45]
MIL-100(Fe)	CO_2/N_2	15	47 *	IAST	[45]
MIL-101(Cr)	CO_2/N_2	15	53 *	IAST	[45]
MIL-102(Cr)	CO_2/N_2	15	41 *	IAST	[45]
MIL-125(Ti)	CO_2/N_2	15	12 *	IAST	[45]
MIL-125(Ti)_NH_2	CO_2/N_2	15	18 *	IAST	[45]
MIL-140A(Zr)	CO_2/N_2	15	10 *	IAST	[45]
MIL-47(V)	CO_2/N_2	15	/		[45]
MIL53(Al)_NH_2	CO_2/N_2	15	877 *	IAST	[45]
MIL-68(Ga)	CO_2/N_2	15	12 *	IAST	[45]
MIL-69(Al)	CO_2/N_2	15	120 *	IAST	[45]
MIL-69(Fe)	CO_2/N_2	15	6 *	IAST	[45]
MIL-91(Al)	CO_2/N_2	15	68 *	IAST	[45]
MIL-91(Ti) HT	CO_2/N_2	15	150 *	IAST	[45]

NaX	CO_2/N_2	15	/		[45]
ScBDC	CO_2/N_2	15	40 *	IAST	[45]
ScBDC_NH$_2$	CO_2/N_2	15	120 *	IAST	[45]
STA-12(Ni)	CO_2/N_2	15	/		[45]
Takeda 5A	CO_2/N_2	15	19 *	IAST	[45]
UiO-66 (Zr)	CO_2/N_2	15	12 *	IAST	[45]
UiO-66(Zr)_Br	CO_2/N_2	15	30 *	IAST	[45]
UiO-66(Zr)_BTeC	CO_2/N_2	15	30 *	IAST	[45]
UiO-66(Zr)_NH$_2$	CO_2/N_2	15	37 *	IAST	[45]
FEFFIVE-Ni-pyr (Dry)	CO_2/N_2	15	∞	GCMC	This work
FEFFIVE-Ni-pyr-SB 4.871% of H_2O	CO_2/N_2	15	∞	GCMC	This work
FEFFIVE-Ni-pyr-SB 9.742% of H_2O	CO_2/N_2	15	8489	GCMC	This work
FEFFIVE-Ni-pyr-SB 14.614% of H_2O	CO_2/N_2	15	1.454	GCMC	This work
FEFFIVE-Ni-pyr-SB 19.485% of H_2O	CO_2/N_2	15	0	GCMC	This work
FEFFIVE-Ni-pyr-SB-FF 4.871% of H_2O	CO_2/N_2	15	∞	GCMC	This work
FEFFIVE-Ni-pyr-SB-FF 9.742% of H_2O	CO_2/N_2	15	∞	GCMC	This work
FEFFIVE-Ni-pyr-SB-FF 14.614% of H_2O	CO_2/N_2	15	9218	GCMC	This work
FEFFIVE-Ni-pyr-SB-FF 19.485% of H_2O	CO_2/N_2	15	4278	GCMC	This work
FEFFIVE-Ni-pyr-SB-FF 24.343% of H_2O	CO_2/N_2	15	0	GCMC	This work

- **** 303 K, remaining at 298K***
- ***FF means derived force field***

Table S11. Comparison of CO_2 working capacities for a series of MOFs and conventional adsorbents at 298 – 303K.

Sample	WC[CO_2/N_2] / $cm^3.cm^{-3}$ (0-1 bar, 303K)	Experimental/Simulation	Ref
CAU-13(Al)	35	Experimental[46]	[46]
CPO-27(Ni)	175	Experimental[47]	[47]
CuBTC	180	Experimental[48]	[48]
MIL-100(Fe)	136.2	Experimental/Simulation[49]	[49]
MIL-101(Cr)	112	Experimental/Simulation[49]	[49]
MIL-102(Cr)	73	Simulation[50]	[50]
MIL-125(Ti)	153	Experimental[51]	[51]
MIL-125(Ti)_NH$_2$	129	Experimental[51]	[51]
MIL-140A(Zr)	69.45	Experimental[52]	[52]
MIL-47(V)	162	Experimental[53]	[53]
MIL53(Al)_NH$_2$	10.1	Experimental[54]	[54]
MIL-68(Ga)	75	Experimental[55]	[55]

MIL-91(Al)	31.5	Experimental/Simulation[56]	[56]
MIL-91(Ti) HT	50.9	Experimental/Simulation	[45]
NaX	70.5	Experimental[57]	[57]
ScBDC	73.1	Experimental/Simulation[58]	[58]
ScBDC_NH$_2$	31.7	Experimental[58]	[58]
STA-12(Ni)	242	Experimental[59]	[59]
Takeda 5A	110	Experimental[59]	[59]
UiO-66(Zr)	175.2	Experimental[60]	[60]
UiO-66(Zr)_BTeC	87.06	Experimental[61]	[61]
UiO-66(Zr)_NH$_2$	125	Experimental[61]	[61]
FEFFIVE-Ni-pyr (Dry)	93.52$^+$	Simulation	This work
FEFFIVE-Ni-pyr-SB 4.871% of H$_2$O	58.70$^+$	Simulation	This work
FEFFIVE-Ni-pyr-SB 9.742% of H$_2$O	38.80$^+$	Simulation	This work
FEFFIVE-Ni-pyr-SB 14.614% of H$_2$O	12.55$^+$	Simulation	This work
FEFFIVE-Ni-pyr-SB 19.485% of H$_2$O	0$^+$	Simulation	This work
FEFFIVE-Ni-pyr-SB-FF 4.871% of H$_2$O	57.53$^+$	Simulation	This work
FEFFIVE-Ni-pyr-SB-FF 9.742% of H$_2$O	46.54$^+$	Simulation	This work
FEFFIVE-Ni-pyr-SB-FF 14.614% of H$_2$O	22.47$^+$	Simulation	This work
FEFFIVE-Ni-pyr-SB-FF 19.485% of H$_2$O	0.86$^+$	Simulation	This work
FEFFIVE-Ni-pyr-SB-FF 24.343% of H$_2$O	0$^+$	Simulation	This work

+298 K, remaining at 303K

References:

1. A. Cadiau, Y . Belmabkhout, K . Adil, PM .Bhatt ,R.S. Pillai,A. Shkurenko,C. Martineau-Corcos, G .Maurin and M .Eddaoudi, *Science.*,2017, **356**, 731-735.

2. J. P. Perdew, *Phys Rev B.*,1986, **33**, 8822-8824.

3. J.P.Perdew, K.Burke, and M. Ernzerhot, *Phys.Rev.Lett*. 1996, **77**, 3865-3868.

4. J. VandeVondele, M. Krack, F. Mohamed, M. Parrinello, T. Chassaing and J. Hutter, *Comput Phys Commun.*,2005, **167**, 103-128.

5. J. VandeVondele and J. Hutter, *J. Chem. Phys.*,2003, **118**, 4365-4369.

6. B. G. Lippert, J. H. Parrinello and Michele, *Mol. Phys.*,1997, **92**, 477-488.

7. G. Lippert, J. Hutter and M. Parrinello, *TheorChem Acc.*,1999, **103**, 124-140.

8. L. Wang, T. Maxisch and G.Ceder, Phys. Rev. B.,2006,73, 195107-195112.

9. W. L. Queen, M. R. Hudson, E. D. Bloch, J. A. Mason, M. I. Gonzalez, J. S. Lee, D. Gygi, J. D. Howe, K. Lee, T. A. Darwish, M. James, V. K. Peterson, S. J. Teat, B. Smit, J. B. Neaton, J. R. Long and C. M. Brown, *Chem. Sci.,* 2014, **5**, 4569–4581.

10. S. Gueddida, S. Lebègue and M. Badawi, *Appl.Surf.Sci.*,2020,**533**,147422.

11. K. Boguslawski, C.R. Jacob and M. Reiher, *J. Chem. Phys.*,2013, **138**, 044111-044127.

12. J. VandeVondele and J. Hutter, *J. Chem. Phys.,*2007, **127**, 114105—114113.

13. T. M. C. Faro, G. P. Thim and M. S. Skaf, *J. Chem. Phys.*, 2010, **132**, 114509-114517.

14. R.S. Pillai and C.H. Suresh, *Phys. Chem. Chem.Phys.*,2019, **21** , 16127–16136.

15. Materials Studio *7.0, Accelrys Software Inc.,* San Diego*, CA 92121, USA.*

16. C. Campana, B. Mussard and T.Woo, *J. Chem. Theory Comput.,*2009, **5**, 2866–2878.

17. G. Opletal, A. Barnard, 2018. PorosityPlus. v1. CSIRO. Software Collection. https://doi.org/10.25919/5b8e0ffa8afaa .

18. L. D. Gelb and K. E. Gubbins, *Langmuir.*, 1998, **15**, 305-308

19. A. K. Rappe, C. J. Casewit, K. S. Colwell, W. A. Goddard and W. M. Skiff, *J. Am. Chem. Soc*.1992, **114**, 10024-10035.

20. S. L. Mayo, B. D. Olafson and W. A. Goddard, *J. Phys. Chem.,*1990, **94**, 8897-8909.

21. J. G. Harris and K.H. Yungt „*J. Phys. chem.* 1995, **99**, 12021–12024

22. M.G. Martin and J.I. Siepmann, *J. Phys. Chem. B*. 1998, **102**, 2569-2577.

23. J. Vekeman, N. Faginas Lago, I. Cuesta, Inmaculada, J. Sanchez-Marín and A. Merás, Computational Science and Its Applications – ICCSA 2018.2018,563-578.

24. S. Murad, K.E. Gubbins, In Computer Modeling of Matter; P. Lykos (Ed.), ACS symposium Series 86; American Chemical Society: Washington DC, 1978, pp. 62.

25. J. L. F. Abascal and C. Vega, *J. Chem. Phys*.2005, **123**, 234505.

26. Z. Hu, Y. Wang, S. Farooq and D. Zhao, *AIChE J.,*2017, **63**, 4103-4114.

27. H. W. Horn, W. C. Swope, J. W. Pitera, J. D. Madura, T. J. Dick, G. L. Hura, and T. Head-Gordon, *J. Chem. Phys*.,2004,**120**,9665-9678.

28. .H. J. C. Berendsen, J. R. Grigera, and T. P. Straatsma, *J. Phys. Chem,* 1987**, 91**, 6269-6271.

29. M.W. Mahoney and W. L. Jorgensen , *J. Chem. Phys*, 2000,**112** ,8910–8922.

30. W L. Jorgensen, J. Chandrasekhar, J D. Madura, R W. Impey, M L. Klein, *J.Chem.Phys*.1983,**79**,926-935.

31. D. Dubbeldam, S. Calero, D. E. Ellis and R. Q. Snurr, *Mol Simulat.*, 2016, **42**, 81-101.

32. D.Y. Peng and D.B. Robinson, *Ind. Eng. Chem. Fundam.*, 1976, **15**, 59-64.

33. T. J. H. Vlugt, E. Garcia-Perez, D. Dubbeldam, S. Ban and S. Calero, *J.Chem. Theory Comput*., 2008, **4**, 1107-1118.

34. Z.Sumer and S. Keskin, *Ind. Eng. Chem. Res*. 2016, **55**, 10404−10419.

35. A.D.Wiersum, J.S.Chang, C.Serre and P.L. Llewellyn, *Langmuir.*, 2013, **29**, 3301–3309.

36. R. Mercado, B. Vlaisavljevich, L.-C. Lin, K. Lee, Y.Lee, J.A. Mason, D.J. Xiao, M.I. Gonzalez, M. T. Kapelewski, J.B Neaton and B. Smit, *J. Phys. Chem. C* .,2016, **120**, 12590−12604

37. N.Chanut, S. Bourrelly, B. Kuchta, C. Serre, J.-S. Chang, P.A. Wright, P.L. Llewellyn, *ChemSusChem.,* 2017, **10**, 1543-1553.

38. Z.J. Chen, K. Adil, L.J. Weselinski, Y. Belmabkhout and M. Eddaoudi, *J. Mater. Chem. A.*,2015, **3**, 6276-6281.

39. P. Nugent, Y. Belmabkhout, S.D. Burd, A.J. Cairns, R. Luebke, K. Forrest, T. Pham, S. Ma, B. Space, L.Wojtas, M. Eddaoudi and M.J. Zaworotko, *Nature*., 2013, **495**, 80-84.

40. D. X. Xue, Y. Belmabkhout, O. Shekhah, H. Jiang, K. Adil, A.J. Cairns and M. Eddaoudi, *J. Am. Chem. Soc.,* 2015, **137**, 5034-5040.

41. O. Shekhah, Y. Belmabkhout, Z. Chen, V. Guillerm, A. Cairns, K. Adil and M. Eddaoudi, Nat. Commun., 2014, **5**, 4228-4231.

42. S.R. Ahrenholtz, C. Landaverde-Alvarado, M. Whiting, S.Y. Lin, C. Slebodnick, E. Marand and A.J. Morris, *Inorg. Chem.*, 2015, **54**, 4328-4336.

43. Q. Yang, S. Vaesen, F. Ragon, A.D. Wiersum, D. Wu, A. Lago, T. Devic, C. Martineau, F. Taulelle, P.L. Llewellyn, H.Jobic, C. Zhong, C.Serre, G. De Weireld and G. Maurin, *Angew. Chem. Int. Edit.*, 2013, **52**, 10316-10320.

44. J. Liu, J.Tian, P.K. Thallapally and B.P. McGrail, *J. Phys. Chem. C.*, 2012, **116**, 9575-9581.

45. V. Benoit, R.S. Pillai, A.Orsi, P. Normand, H.Jobic, F.Nouar, P.Billemont, E. Bloch, S.Bourrelly, T. Devic, P.A. Wright, G. de Weireld, C.Serre, G.Maurin and P.L. Llewellyn, *J. Mater. Chem. A.*, 2016, **4**, 1383-1389.

46. F.Niekiel, J.Lannoeye, H.Reinsch, A.S. Munn, A.Heerwig, I.Zizak, S.Kaskel, R.I. Walton, D. de Vos, P.L. Llewellyn, A.Lieb, G. Maurin and N. Stock, *Inorg. Chem.*, 2014, **53**, 4610-4620.

47. W.L. Queen, M.R. Hudson, E.D. Bloch, J.A. Mason, M.I. Gonzalez, J.S. Lee, D.Gygi, J.D. Howe, K. Lee, T.A.Darwish, M. James, V.K. Peterson, S.J. Teat, B.Smit, J.B.Neaton, J.R. Long and C.M. Brown, *Chem. Sci.,* 2014, **5**, 4569-4581.

48. L. Grajciar, A.D. Wiersum, P.L. Llewellyn, J.S. Chang and P. Nachtigall, *J. Phys. Chem. C.,* 2011, **115**, 17925-17933.

49. P.L. Llewellyn, S.Bourrelly, C.Serre, A.Vimont, M.Daturi, L.Hamon, G. De Weireld, J.S.; Chang, D.Y. Hong, Y.Kyu Hwang, S.HwaJhung and G.Férey, *Langmuir.*, 2008, **24**, 7245-7250.

50. D.Damasceno Borges, M.Prakash, N.A.Ramsahye, P.L. Llewellyn, S.Surblé, P.Horcajada, C.Serre and G.Maurin, *Mol. Simulat.*, 2015, **41**, 1357-1370.

51. S. Vaesen V.Guillerm, Q. Yang, A.D.Wiersum, B.Marszalek, B. Gil, A.Vimont, M.Daturi, T.Devic, P.L. Llewellyn, C.Serre, G.Maurin and G. De Weireld, *Chem. Commun.*, 2013, **49**, 10082-10084.

52. G.D. Pirngruber, L.Hamon, S. Bourrelly, P.L. Llewellyn, E. Lenoir, V. Guillerm, C.Serre and T.Devic, *ChemSusChem.,* 2012, **5**, 762-776.

53. P.L. Llewellyn, S.Bourrelly, C. Vagner, N. Heymans, H. Leclerc, A.houfi, P.Bazin, A.Vimont, M.Daturi, T.Devic, C.Serre, G. De Weireld and G.Maurin, *J. Phys. Chem. C.*, 2013, **117**, 962-970.

54. S.Couck, J.F.Denayer, G.V. Baron, T. Remy, J.Gascon and F. Kapteijn, *J. Am. Chem. Soc.*, 2009, **131**, 6326-6327.

55. Q. Yang, S.Vaesen, M. Vishnuvarthan, F.Ragon, C.Serre, A.Vimont, M. Daturi, G. De Weireld and G.Maurin, *J. Mater. Chem.*, 2012, **22**, 10210-10220

56. P.L. Llewellyn, M. Garcia-Rates, L.Gaberova, S.R. Miller, T.Devic, J.C.Lavalley, S.Bourrelly, E. Bloch, Y.Filinchuk, P.A. Wright, C.Serre, A.Vimont and G.Maurin, *J. Phys. Chem. C.*, 2015, **119**, 4208-4216.

57. A.D.Wiersum, J.S. Chang, C.Serre and P.L. Llewellyn, *Langmuir.*, 2013, **29**, 3301-3309.

58. R.S.Pillai, V. Benoit, A.Orsi, P.L. Llewellyn, P.A. Wright and G.Maurin, *J. Phys. Chem. C.*,2015, **119**, 23592-23598.

59. S.R. Miller, G.M. Pearce, P.A. Wright, F.Bonino, S.Chavan, S.Bordiga, I.Margiolaki, N.Guillou, G.Férey, S.Bourrelly and P.L. Llewellyn, *J. Am. Chem. Soc.*, 2008, **130**, 15967-15981.

60. Q.Yang, A.D.Wiersum, H.Jobic, V. Guillerm, C. Serre, P.L. Llewellyn and G. Maurin, *J. Phys. Chem. C.,* 2011, **115**, 13768-13774..

61. Q.Yang, A.D.Wiersum, P.L. Llewellyn, V. Guillerm, C.Serred and G.Maurin, *Chem. Commun.,* 2011, **47**, 9603-9605.